Monthly Notices
of the
ROYAL ASTRONOMICAL SOCIETY

MNRAS **469,** S787–S803 (2017)
Advance Access publication 2017 October 9

doi:10.1093/mnras/stx2534

Sulphur isotope mass-independent fractionation observed in comet 67P/Churyumov–Gerasimenko by *Rosetta*/ROSINA

U. Calmonte,[1★] K. Altwegg,[1,2★] H. Balsiger,[1] J.-J. Berthelier,[3] A. Bieler,[1,4] J. De Keyser,[5] B. Fiethe,[6] S. A. Fuselier,[7,8] S. Gasc,[1] T. I. Gombosi,[4] L. Le Roy,[1] M. Rubin,[1★] T. Sémon,[1] C.-Y. Tzou[1] and S. F. Wampfler[2]

[1]*Physikalisches Institut, University of Bern, Sidlerstrasse 5, CH-3012 Bern, Switzerland*
[2]*Center for Space and Habitability, University of Bern, Sidlerstrasse 5, CH-3012 Bern, Switzerland*
[3]*LATMOS, 4 Avenue de Neptune F-94100 Saint-Maur, France*
[4]*Department of Atmospheric, Oceanic and Space Sciences, University of Michigan, 2455 Hayward, Ann Arbor, MI 48109, USA*
[5]*Royal Belgian Institute for Space Aeronomy (BIRA-IASB), Ringlaan 3, B-1180 Brussels, Belgium*
[6]*Institute of Computer and Network Engineering (IDA), TU Braunschweig, Hans-Sommer-Strasse 66, D-38106 Braunschweig, Germany*
[7]*Space Science Division, Southwest Research Institute, 6220 Culebra Road, San Antonio, TX 78228, USA*
[8]*Department of Physics and Astronomy, University of Texas at San Antonio, One UTSA Circle, San Antonio, TX 78249, USA*

Accepted 2017 September 26. Received 2017 September 26; in original form 2017 April 18

ABSTRACT

The knowledge about sulphur isotopic fractionation in volatile cometary species is limited as only measurements in five comets have been done and only for $^{34}S/^{32}S$. The lack of information about the fractionation of $^{33}S/^{32}S$ makes it impossible to compare them with what is known from refractories. We present results of $^{34}S/^{32}S$ and for the first time $^{33}S/^{32}S$ isotopic ratio in H_2S, OCS, and CS_2 in the coma of comet 67P/Churyumov–Gerasimenko. Observations used for this study were performed with *Rosetta* Orbiter Spectrometer for Ion and Neutral Analysis/Double Focusing Mass Spectrometer during 2014 October and 2016 May. Bulk isotopic $^{33}S/^{32}S$ and $^{34}S/^{32}S$ ratios derived from these three species yield $\delta^{33}S = (-302 \pm 29)‰$ and $\delta^{34}S = (-41 \pm 17)‰$, respectively. The observed isotopic fractionation is significantly different from the assumed Solar system standard [Vienna-Canyon Diablo Troilite (V-CDT)] and all other reported values for Solar system objects, except other comets. Furthermore, we show that neither mass-dependent nor mass-independent fractionation due to photodissociation as it has been observed in recent laboratory studies can be the cause of the significant depletion compared to Solar system standard. In addition, we conclude that there seems to be an intrinsic difference in sulphur isotopic fractionation in cometary volatiles and refractories while the difference between molecules is most likely due to different chemical pathways. The significant fractionation of sulphur isotopes together with a high D_2O/HDO versus HDO/H_2O and non-solar isotopic ratio for xenon as well as for Si point towards a non-homogeneously mixed protosolar nebula.

Key words: comets: general – comets: individual: 67P/Churyumov–Gerasimenko.

1 INTRODUCTION

Rosetta is a mission of the European Space Agency (ESA) with the aim to characterize Jupiter-family comet 67P/Churyumov–Gerasimenko (hereafter 67P) *in situ*. *Rosetta* followed the comet from a heliocentric distance of more than 3.6 au to perihelion and finally away again from the Sun to almost 3.8 au. One of the science goals of *Rosetta* was the determination of the elemental, isotopic, and molecular composition of the cometary material. Most of the composition measurements during the mission, especially isotopic measurements, were done from the *Rosetta* orbiter in the coma, by the instrument ROSINA (*Rosetta* Orbiter Spectrometer for Ion and Neutral Analysis; Balsiger et al. 2007) in the case of volatiles and by COSIMA (COmetary Secondary Ion Mass Analyser) in the case of dust. A limited number of measurements have been performed directly on the nucleus by the COSAC (Goesmann et al. 2015) and Ptolemy (Wright et al. 2015) instruments. ROSINA consists of the Double Focusing Mass Spectrometer (DFMS), the Reflectron-type Time-Of-Flight mass spectrometer and the COmet Pressure

★ E-mail: ursina.calmonte@space.unibe.ch (UC); kathrin.altwegg@space.unibe.ch (KA); martin.rubin@space.unibe.ch (MR)

© 2017 The Author(s)
Published by Oxford University Press on behalf of the Royal Astronomical Society

source: https://doi.org/10.7892/boris.111863 | downloaded: 25.4.2024

Downloaded from https://academic.oup.com/mnras/article-abstract/469/Suppl_2/S787/4411814
by Universitaetsbibliothek Bern user
on 20 February 2018

Table 1. Absolute isotope ratios of international standards.

Standard	Ratio	Accepted value ($\times 10^{-5}$)	Reference
SVMOW	$^{18}O/^{16}O$	2005.20 ± 0.45	Werner & Brand (2001)
SVMOW	$^{17}O/^{16}O$	379.9 ± 0.8	Werner & Brand (2001)
V-PDB	$^{13}C/^{12}C$	11 180.2 ± 2.8	Werner & Brand (2001)
V-CDT	$^{34}S/^{32}S$	44 150.9 ± 11.7	Ding et al. (2001)
V-CDT	$^{33}S/^{32}S$	7877.24	Ding et al. (2001)

Sensor (COPS). The composition of the coma, including dust and gas, depends on the actual composition of the nucleus and the physical and chemical processes involved in the desorption, sublimation and transport of the material into the coma.

ROSINA has been sampling the volatiles in the coma throughout the mission. ROSINA observations revealed some remarkable links to pre-solar ices, including elevated D/H ratios in singly and doubly deuterated water (Altwegg et al. 2015; Altwegg 2017), a remarkable abundance of molecular oxygen, O_2, well correlated to H_2O and possibly inherited from irradiated interstellar ice grains (Bieler et al. 2015), and xenon isotopic ratios different from solar (Marty 2017).

Among the most abundant species in the volatile phase are sulphur-bearing molecules (Calmonte et al. 2016). The amounts observed using ROSINA DFMS were high enough that several of the isotopologues could be detected and analysed. Sulphur has four stable isotopes: ^{32}S, ^{33}S, ^{34}S, and ^{36}S with relative abundances of 94.93 per cent, 0.76 per cent, 4.29 per cent, and 0.02 per cent based on the standard derived from the Vienna-Canyon Diablo Troilite (V-CDT; Ding et al. 2001). Most sulphur-bearing species are formed on dust grains; some of them are then formed by radiolysis by cosmic rays (Woods et al. 2015 and references therein).

Objects in the Solar system show varying relative abundances of sulphur isotopes. The few comets, for which we have isotopic ratios, are no exception, even though the measurements prior to *Rosetta* are limited to the more abundant minor isotope ^{34}S. In this work, we present the measurements of isotopologues by ROSINA DFMS of an extended list of sulphur-bearing molecules and report on the ^{33}S abundances where possible. These results are then compared to the ratios measured in other objects in the Solar system and laboratory investigations of fractionation processes occurring in the early Solar system.

The first section of the paper will review the observations of sulphur isotopes in chondrites and pre-solar material as well as earlier observations obtained at comets. The next section is dedicated to the description of the ROSINA DFMS, the details of the data treatment, and the analysis. In the third section, the results for the individual molecules are presented and followed by discussion and conclusions.

2 SULPHUR MASS FRACTIONATION IN SOLAR SYSTEM BODIES

There are two conventions how to display isotope fractionation and here we show how they are linked. Usually sulphur isotopic ratios in cometary gas are presented as follows: $^{32}S/^{33}S$ and $^{32}S/^{34}S$ whereas in meteoritic studies mass fractionation is given as deviation from a standard value (V-CDT, Table 1) in per mile:

$$\delta^{33}S = [(^{33}S/^{32}S)_{sample}/(^{33}S/^{32}S)_{standard} - 1] \cdot 1000$$

and

$$\delta^{34}S = [(^{34}S/^{32}S)_{sample}/(^{34}S/^{32}S)_{standard} - 1] \cdot 1000.$$

Table 2. Laboratory measurements of photodissociation-related fractionation in H_2S, CS_2, and OCS.

Species	$\delta^{34}S/\delta^{33}S$	Reference
H_2S	0.64–0.7	Zmolek et al. (1999)
CS_2	0.485 ± 0.005	Chakraborty et al. (2013)
OCS	0.534 ± 0.005	Lin et al. (2011)

2.1 Laboratory measurements of sulphur isotope fractionation

Concerning mass-independent sulphur fractionation (MIF), only a few studies have been done to date (Table 2). The impact on the sulphur isotope ratio has been studied for photopolymerization by solar irradiation in the gas phase of $^{12}CS_2$ and $^{13}CS_2$ to $(^{12}CS_2)_x$ leading to a fractionation of $\delta^{34}S = 45.85$ ‰, $\delta^{33}S = 28.31$ ‰, and $\delta^{36}S = 37.6$ ‰ resp. to $(^{13}CS_2)_x$ leading to a fractionation of $\delta^{34}S = 32.48$ ‰, $\delta^{33}S = 16.98$ ‰, and $\delta^{36}S = 56.7$ ‰ (Zmolek et al. 1999).

For H_2S photodissociation by solar vacuum UV photons, experiments have been done by Chakraborty et al. (2013) at four different wavelengths including Lyman α in the range of 2×10^{-2} to 0.2 mbar and different photolysis time resulting in an MIF for Lyman α of $\delta^{33}S = (0.27–6.94)$ ‰, $\delta^{34}S = (1.95–13.87)$ ‰, and $\delta^{34}S = (5.95–26.60)$ ‰.

Recently, the dependence of pressure and 'third body' effects during photolysis of SO_2 has been studied by Masterson, Farquhar & Wing (2011). With a D_2 lamp providing a broad-band UV continuum peaking at 200 nm, gas mixtures of SO_2 and He, with mixing ratios between 1:0 and 1:26, have been irradiated at different pressures. For SO_2, only the investigated pressure range was 20–880 mbar and for mixtures with He the range was 125–700 mbar. The MIF with only SO_2 leads to $\delta^{34}S = 127.42–160.98$ ‰ and $\delta^{33}S = 65.80–106.82$ ‰ , while the mixture of SO_2 and He leads to $\delta^{34}S = 133.55–177.55$ ‰ and $\delta^{33}S = 71.92–102.56$ ‰. Another lab experiment showed that photolysis of OCS produces very little isotope fractionation, less than 10 ‰ (Lin, Sim & Ono 2011).

2.2 Meteorites

Fig. 1 gives a compilation of results from meteoritic studies. Generally, deviations from the standard V-CDT are low, less than 10‰, and the deviations can be very well explained by mass-dependent fractionation. However, for silicon carbide (SiC) grains, which represent most probably pre-solar material, sulphur isotopic deviations from the standard are much more pronounced reaching a few hundred ‰. A compilation of results from the literature is shown in Fig. 2. For a more extensive review, see Appendix A.

2.3 Comets

So far measurements of $^{32}S/^{34}S$ have been reported for five comets of different dynamical origin in different molecules, and were determined except for 1P/Halley by remote sensing (Table 3). While the ratio for S^+ in comet 1P/Halley and in CS in the comets C/1995 O1 Hale–Bopp, C/2014 Q2 Lovejoy, and C/2012 F6 Lemmon is compatible with solar, H_2S in C/1995 O1 Hale–Bopp is depleted in ^{32}S. However, error bars are large and the difference in measurement methods and the fact that the isotopic ratios have been measured *in situ* in CS_2, but remotely in CS, make a comprehensive comparison difficult. In addition, in comet 17P/Holmes, the detection of $H_2^{34}S$ has been reported (Biver et al. 2008); however, it is solely stated that

Downloaded from https://academic.oup.com/mnras/article-abstract/469/Suppl_2/S787/4411814
by Universitaetsbibliothek Bern user
on 20 February 2018

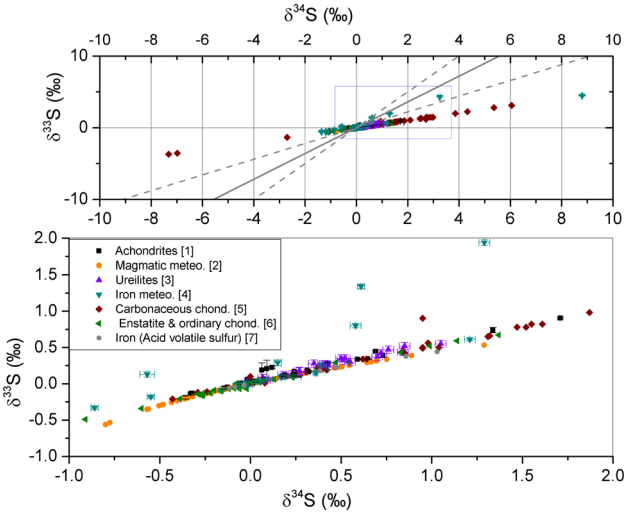

Figure 1. Sulphur three-isotope graph comparing deviation from V-CDT in different types of meteorites. The upper graph shows the full scale of deviation of sulphur in meteorites in general while the bottom graph shows the section of a few ‰ around the centre of origin. [1] Rai, Jackson & Thiemens (2005), [2] Antonelli et al. (2014), [3] Farquhar, Jackson & Thiemens (2000), [4] Gao & Thiemens (1991), [5] Gao & Thiemens (1993a), [6] Gao & Thiemens (1993b), [7] Franz, Farquhar & Irving (2010), Hoppe, Lodders & Fujiya (2015).

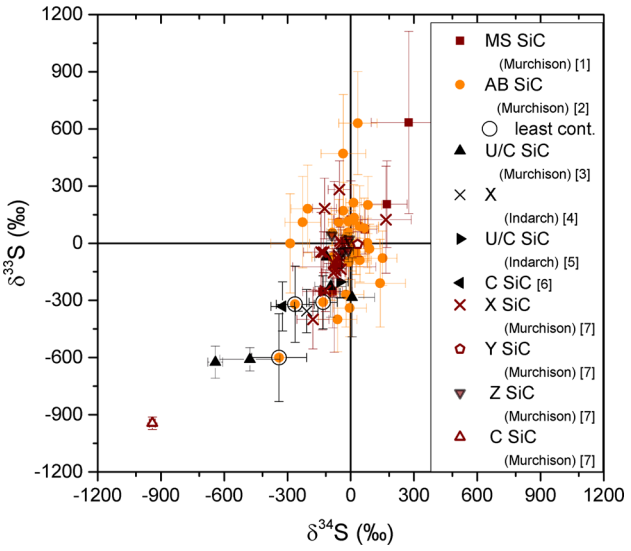

Figure 2. Three-isotope graph of sulphur isotopic ratios relative to V-CDT in SiC grains from the meteorites Murchison and Indarch. Hosting meteorite is given in brackets when known. [1] Hoppe et al. (2015), [2] Fujiya et al. (2013), [3] Hoppe, Fujiya & Zinner (2012), [4] Gyngard, Nittler & Zinner (2010), [5] Orthous-Daunay et al. (2012), [6] Gyngard et al. (2010), [7] Xu et al. (2015).

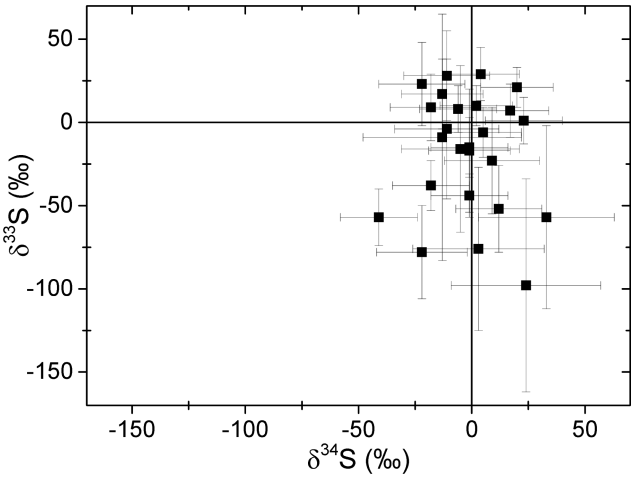

Figure 3. Sulphur isotopic fractionation with respect to V-CDT in comet Wild 2 dust impactor samples collected by *Stardust* mission (Heck et al. 2012).

the resulting isotopic ratio of $^{32}S/^{34}S$ is in agreement with terrestrial value.

Besides the attempts to sample the coma by *in situ* measurements and via remote sensing, the National Aeronautics and Space Administration (NASA) *Stardust* mission collected in 2004 January the first samples of cometary matter and brought them back to Earth in 2006. The samples were collected during a fly-by at 234 km distance from Jupiter-family comet Wild 2. They were collected with the Aerogel Sample Collectors which consisted mostly of a silica aerogel and ≈15 per cent aluminium (frame to hold aerogel). Impact craters contained melted and sometimes unmelted residues of the impactor (Brownlee et al. 2006). From those 24 dust impactors in the aluminium frame, the residues were analysed for their four sulphur isotopic composition (Heck, Hoppe & Huth 2012). In this data set, only one impact crater residue showed a small depletion of ^{33}S and ^{34}S [$\delta^{33}S = (-41 \pm 17)$‰ and $\delta^{34}S = (-57 \pm 17)$‰, respectively] while the rest were within 2σ of bulk meteorite data as can be seen by comparing Figs 3 and 1. Heck et al. (2012) stated that the small anomaly might be the result of a mixture between a small pre-solar grain and a larger grain formed in the Solar system and that the relatively large uncertainties are due to topographic effects of the residues and possible impact fractionation.

3 DATA ACQUISITION AND REDUCTION

All data used for this study have been acquired with ROSINA DFMS in high resolution mode. Distance of *Rosetta* is given with reference to the comet centre (Scholten et al. 2015) and time stamps in UTC. For determination of sulphur isotopic ratios, only species (e.g. H_2S) were taken into account which are unlikely to be a fragment (e.g. HS) due to the ionization process in DFMS. In this section, a brief

Table 3. Sulphur isotope ratios reported in cometary gas phase prior to *Rosetta*.

$^{32}S/^{34}S$	$\delta^{34}S$	Comet	Species	Method	Reference
23 ± 6	−15 ± 257	1P – Halley	$^{34}S^+$	Mass spec (Giotto)	Altwegg (1995)
27 ± 3	−161 ± 93	C/1995 O1 – Hale–Bopp	$C^{34}S$	(Sub-)mm spec (JCMT)	Jewitt et al. (1997)
16.5 ± 3.5	372 ± 310	C/1995 O1 – Hale–Bopp	$H_2{}^{34}S$	(Sub-)mm spec (30 m IRAM)	Crovisier et al. (2004)
24.7 ± 3.5	−83 ± 130	C/2014 Q2 – Lovejoy	$C^{34}S$	(Sub-)mm spec (30 m IRAM)	Biver et al. (2016)
20 ± 5	132 ± 283	C/2012 F6 – Lemmon	$C^{34}S$	(Sub-)mm spec (30 m IRAM)	Biver et al. (2016)

Downloaded from https://academic.oup.com/mnras/article-abstract/469/Suppl_2/S787/4411814
by Universitaetsbibliothek Bern user
on 20 February 2018

summary on the working principle of DFMS and the data reduction will be given as both have been presented in more detail in Le Roy et al. (2015) and Calmonte et al. (2016).

3.1 Double Focusing Mass Spectrometer (DFMS)

For isotopic measurements, ROSINA DFMS is used because of its high mass resolution of $m/\Delta m = 9000$ (at full width half max) at mass-to-charge ratio 28 u/e and its high dynamic range of 10^{10} (Balsiger et al. 2007). Operation principles of DFMS allow the acquisition of single mass spectra covering about ±0.2 u/e around the selected integer mass-to-charge ratio. In general, it takes up to 40 min to cover the range from 13 to 100 u/e with a standard mode. DFMS consists of three main parts: ion source, mass analyser, and detector head. Neutral particles entering the ion source are ionized by electron impact ionization at 45 eV. The ionized particles are then extracted and guided to the mass analyser that consists of an electrostatic analyser and a magnet in the Nier–Johnson geometry. Thus, only ions with a certain energy range (E_{ESA} ±1 per cent) can pass the electrostatic analyser to enter the magnet for the mass-to-charge based separation. After this step, the ion beam impinges on one of DFMS's three detectors. Here only the position-sensitive multi-channel plate detector has been used (hereafter referred to as MCP/LEDA). It consists of two parts, a multi-channel plate (MCP) followed by a linear electron detector array (LEDA). The MCP consists of two 0.3 mm thick plates mounted in a chevron configuration with an inclination of 13°. The LEDA consists of two independent rows (Row A, Row B) with 512 anodes each. In order to measure secondary electrons produced by the MCP, the anodes are pre-charged with a small charge, which leads to a well-studied offset in the spectra. The LEDA measures in analogue mode which is converted to a digital signal. A more detailed discussion on the MCP-LEDA was done by Berthelier et al. (2002) and Nevejans et al. (2002). A requirement was that DFMS can measure in a wide range of densities with constant characteristics. This is achieved by automatic gain adjustment of the detector. There are 16 different defined potentials called gain steps with known amplifications calibrated in the lab.

3.2 Data acquisition

Rosetta accompanied comet 67P for 790 d before soft-landing at the comet end of 2016 September. During two periods within the 790 d, conditions were such that H_2S and CS_2 had a sufficient signal to determine the $^{33}S/^{32}S$ and $^{34}S/^{32}S$ ratios. In the following, the observation geometry of the two periods will be outlined.

During 2014 October, *Rosetta* was at 10 km distance from the centre of the comet for almost 14 d which is equivalent to almost 28 cometary days in this configuration. The majority of the data were acquired with a standard high-resolution mode that allowed sequential measurements from mass-to-charge ratio 13 u/e up to 100 u/e in about 40 min. *Rosetta* was in a terminator orbit, between −50° and 50° latitude. The subsolar latitude was at that time around 40° north. The uppermost panel of Fig. 4 shows signal strength of H_2S, OCS, and CS_2 in arbitrary units. The two following panels show sub-satellite latitude and distance of *Rosetta* from 67P's centre of mass and heliocentric distance of the comet, respectively. For H_2S and CS_2, signal strength during the majority of the period was sufficient to detect the minor isotopologues. 38 data sets were analysed for H_2S between 20.10.2014 01:30 and 26.10.2014 03:00. Around the time of the highest intensity during this period of H_2S on October 25 for CS_2, 12 data sets acquired between

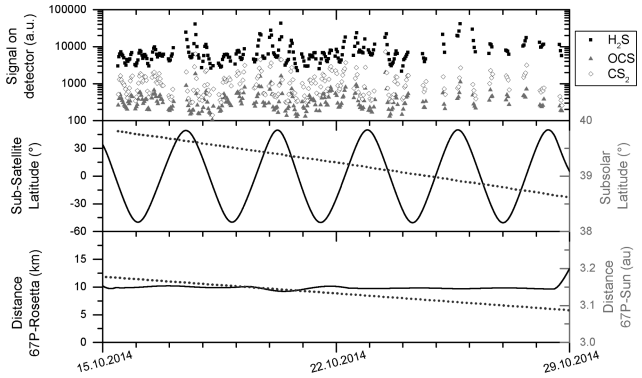

Figure 4. Compilation of *Rosetta*'s orbital parameters and signal strength of H_2S, OCS, and CS_2 in the vicinity of 67P during 2014 October. The uppermost panel shows the signal strength in arbitrary units, the middle panel shows sub-satellite (solid line) and solar latitude (dotted line), and the bottom panel shows the heliocentric (dashed line) and cometocentric distances (solid line) of 67P and *Rosetta*, respectively (coordinate system; Scholten et al. 2015).

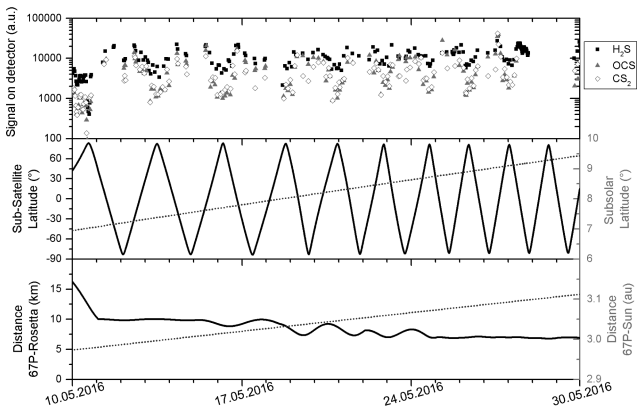

Figure 5. Compilation of *Rosetta*'s orbital parameters and signal strength of H_2S, OCS, and CS_2 in the vicinity of 67P during 2016 May. The uppermost panel shows the signal strength in arbitrary units, the middle panel shows sub-satellite (solid line) and solar latitude (dashed line), and the bottom panel shows the changes in heliocentric (dashed line) and cometocentric (solid line) distances of 67P and *Rosetta*, respectively (coordinate system; Scholten et al. 2015).

23.10.2014 18:10 and 26.10.2014 03:50 had a statistically significant peak maximum for the least common isotopologues. In order to increase the sample size, 13 data sets acquired between 21.10.2014 19:20 and 22.10.2014 21:10, for which the signal was high enough, were added to the analysis. Unfortunately, the signal strength for OCS was only high enough to detect the minor isotopologues during the local maximum. In total, five data sets were analysed and a preliminary value for $\delta^{34}S$ could be determined. A detailed list of the used data sets of all species can be found in Appendix B.

During 2016 May, *Rosetta*'s orbit was bound to be as close as flight operations would allow and thus the measured signals were again comparable to the first selected period (see Fig. 5). This was 2 months after equinox with the subsolar latitude still close to the equator, but at northern latitudes (5°–10°). However, for OCS the signal strength was higher than during the first period, thus making it possible to determine $\delta^{33}S$ as well. Unlike in 2014 October, it was possible in 2016 May to sample the regions above the poles.

Downloaded from https://academic.oup.com/mnras/article-abstract/469/Suppl_2/S787/4411814
by Universitaetsbibliothek Bern user
on 20 February 2018

Rosetta spent 3 weeks within 10–7 km to the centre of the comet sampling latitudes from −90° to 90°. The heliocentric distances were similar in 2014 October and 2016 May, around 3 au. For H_2S, all spectra between 16.05.2016 10:20 and 28.05.2016 03:46 which were acquired with the same MCP settings could be used for this study resulting in 24 data points. For CS_2, 34 data sets could be used from the period 24.05.2016 07:20 to 30.05.2016 23:55. Again for OCS it was more difficult due to lower signal. Only 15 spectra between 12.05.2016 13:14 and 28.05.2016 03:50 had statistically usable signals.

3.3 Data reduction

Data reduction of DFMS MCP-LEDA data requires the following steps: subtraction of the LEDA offset, conversion from analogue-to-digital counts to ions per spectrum, and conversion from pixel position on the LEDA to mass-to-charge ratio. Detailed descriptions on this and how species are identified in a spectra can be found in the works by Le Roy et al. (2015) and Calmonte et al. (2016).

In order to minimize errors, only spectra were used where the gain of the detector remained constant for all isotopologues of one species. In addition, the gain of the individual pixels of the detector was corrected for the degradation over the course of the mission. This was done by regular calibration measurements of the individual pixel gain. The data have also been corrected for the changing sensitivity of DFMS with mass-to-charge ratio. As an empirical correction factor, deduced from calibration work, the sensitivity S is related to mass-to-charge m/Q as $S \sim (m/Q)^{-0.8}$.

Each individual peak can be approximated by the sum of two Gaussian functions, with the second having an amplitude of roughly 10 per cent of the first one and being roughly three times broader. To derive the number of ions per spectrum per species in general, the data have to be fitted due to overlap between different species. This has been done with a least-squares fit using the Levenberg–Marquardt algorithm. The fits were performed under the following constraints. All peaks on the same mass/charge channel share the same amplitude (area) ratio and the same widths of the two Gaussian functions. The peak centres are known from the exact mass of the species. Spacecraft contamination (Schläppi et al. 2010) was neglected as the only species present before the encounter with 67P was H_2S at a very minor level (Calmonte et al. 2016).

3.4 Uncertainties

The uncertainties on the sulphur isotopic ratios include the statistical uncertainties given by the ion statistics, the uncertainty on the determined pixel gain factors, the uncertainty of the sensitivity correction and the uncertainty introduced by the least-squares fit. In the following, their contributions to the overall uncertainty will be discussed in detail. The statistical uncertainty is given by the square root of the number of detected ions per spectrum. For studies of most gases in the coma of 67P, this term is $\ll$1 per cent, though for small signals of minor S-bearing gases it has to be taken into account. As has been explained (Section 3.3), the MCP degraded as a function of time, depending on the number of impacting ions, which results in a change in the individual pixel gain of the MCP-LEDA. Calibration measurements to determine these factors were performed regularly but have some uncertainty. In the best case, isotopologues fall on to the same pixel and any associated uncertainty in the ratio vanishes. This is almost the case for CS_2. For H_2S, the different isotopologues fall on different pixels as the mass difference

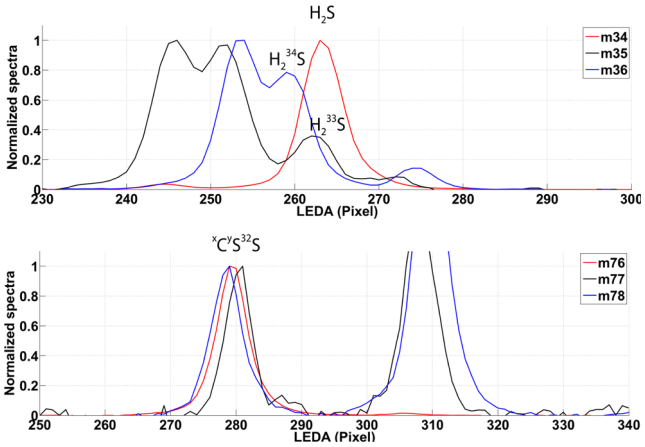

Figure 6. Position of isotopologues of a species on the MCP-LEDA. The spectra have been normalized to the highest intensity in the spectra and only the peaks of interest have been labelled (for more details, see Fig. 7). The top panel shows the spectra with the isotopologues of H_2S with ^{32}S in red, ^{33}S in black, and ^{34}S in blue, respectively, as a function of the pixel number. The bottom panel shows the same type of figure for CS_2. Comparing the pixel difference between major and minor isotopologues for H_2S and CS_2, it can be seen that in the case of the latter the difference is almost zero while for H_2S it can be up to 6 pixels.

between them is not exactly 1.000 u. In the top panel of Fig. 6, the spectra of one set of H_2S isotopologue measurements are plotted as a function of pixel number. To simplify the comparison, the spectra have been normalized to the highest peak present. It can be seen that the difference in position on the LEDA between H_2S and $H_2{}^{33}S$ is about 2–3 pixels while for $H_2{}^{34}S$ it is about 5–6 pixels. In contrast, the difference in position between the isotopologues of CS_2 is at maximum 1 pixel as shown in the bottom panel. Based on the pixel gain curves used for this study and the difference in peak position, the maximum bias introduced by correcting for the individual pixel gain factors is estimated for H_2S, OCS, and CS_2 to be 7 per cent, 5 per cent, and 3 per cent, respectively. The intensities have also been corrected for the mass-dependent sensitivity of the instrument (Balsiger et al. 2007) and the corresponding uncertainties have been taken into account.

The uncertainty introduced by the least-squares fit depends on the degree of overlap and the relative abundances of overlapping species. Based on the spectra, the following uncertainties have been estimated. In the case of H_2S, the fit uncertainties are assumed to be highest as there are overlaps of the peak of interest with at least one peak (see Fig. 7). This results in a fit uncertainty of 15 per cent, 20 per cent, and 10 per cent for $H_2{}^{32}S$, $H_2{}^{33}S$, and $H_2{}^{34}S$, respectively. In the case of OCS, less interfering peaks are present. On mass-to-charge 60 u/e there might be a peak at 10 per cent while on mass-to-charge ratio 62 u/e no interfering peak seems to be present. The fit uncertainties for $OC^{32}S$, $OC^{33}S$, and $OC^{34}S$ are estimated to be 10 per cent, 30 per cent, and 5 per cent, respectively. In the case of CS_2, there are interferences for the minor isotopologues with other species present. The fit uncertainties for $C^{32}S_2$, $C^{33}S_2$, and $C^{34}S_2$ are estimated to be 5 per cent, 20 per cent, and 10 per cent, respectively. Error bars are due to Gaussian error propagation and are calculated in the δ notation as follows:

$$s_{\delta^{3i}S} = \frac{s_{(^{3i}S/^{32}S)}}{(^{3i}S/^{32}S)_{Standard}} \cdot 1000 \qquad i = 3, 4$$

whereas $s_{\delta^{3i}S}$ is the uncertainty of $\delta^{3i}S$ and $s_{(^{3i}S/^{32}S)}$ the uncertainty of the measured ratio.

Downloaded from https://academic.oup.com/mnras/article-abstract/469/Suppl_2/S787/4411814
by Universitaetsbibliothek Bern user
on 20 February 2018

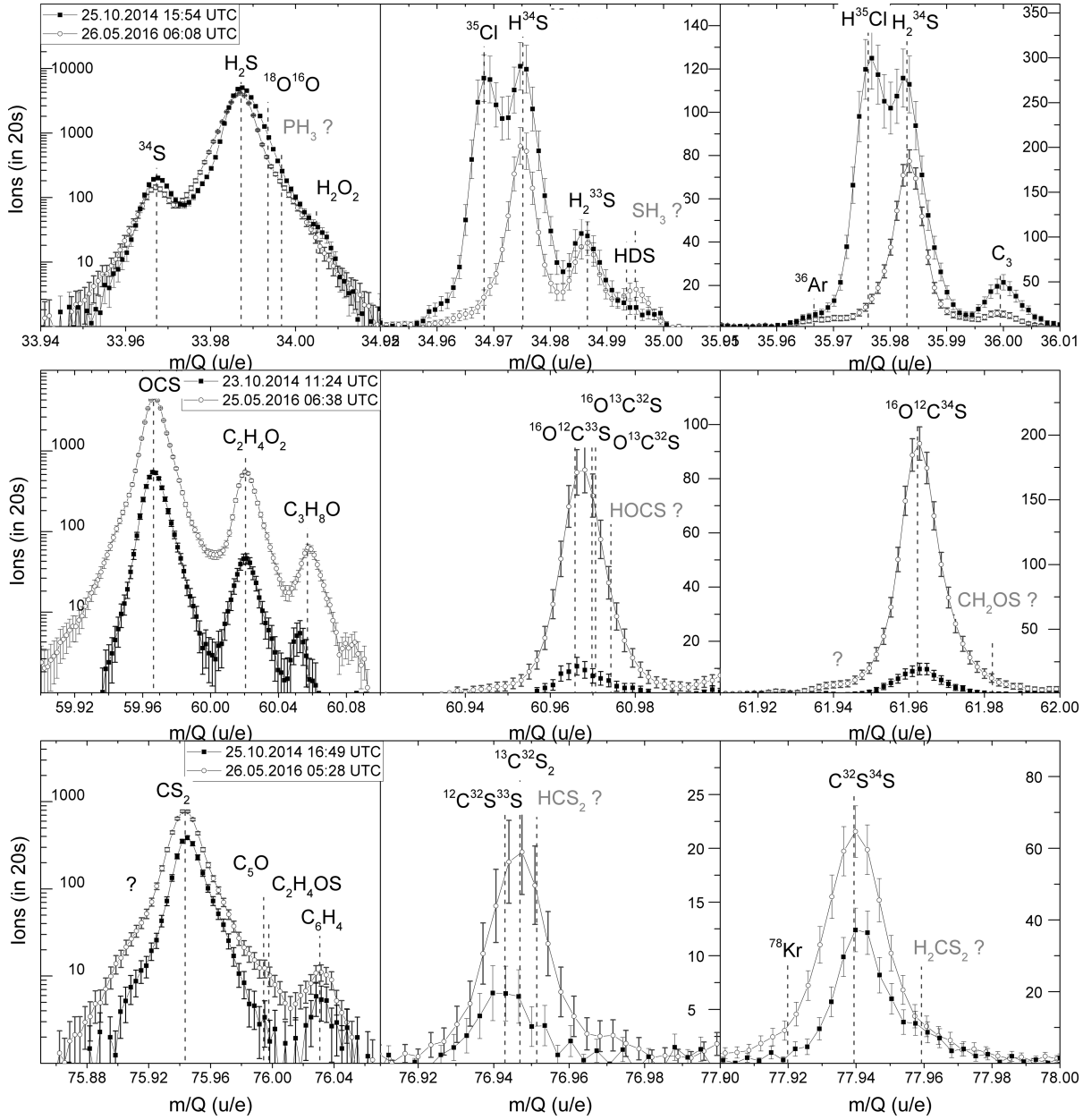

Figure 7. Example spectra of mass-to-charge 34–36 u/e, 60–62 u/e, and 76–78 u/e showing, among others, the isotopologues of H_2S, OCS, and CS_2 measured during 2014 October and 2016 May. Identified species are labelled in black while others are labelled in grey. Error bars solely represent statistical uncertainties.

4 RESULTS

In this section, we first present some typical spectra containing signals from the isotopologues of H_2S, OCS, and CS_2 and in addition interferences due to other species. Then for H_2S, OCS, and CS_2, the isotopic ratios are presented individually. The derived isotopic ratios in these molecules are given as deviation from the standard V-CDT. For H_2S and CS_2, it was possible to determine $\delta^{33}S$ and $\delta^{34}S$ for both selected periods in 2014 November and 2016 May, respectively. In the case of OCS, $\delta^{33}S$ and $\delta^{34}S$ could be determined for 2016 May but the signal strength in 2014 November was just enough to determine $\delta^{34}S$. In this study, mean isotopic ratios are presented by $\bar{x} \pm \sigma_{\mathrm{mean}}$ ($1\sigma_{\mathrm{single}}$), where $\bar{x}$ denotes the mean value, σ_{mean} the uncertainty of the mean and σ_{single} the mean standard deviation of the single measurements. For comparison of the mean value with V-CDT, the uncertainty σ_{mean} is crucial.

4.1 Inventory of species

Fig. 7 shows a compilation of typical spectra of mass-to-charge (m/Q) 34–36 u/e, 60–62 u/e, and 76–78 u/e which contain the isotopologues of H_2S, OCS, and CS_2. Identified species are labelled in black while not yet confirmed species are labelled in grey. The same spectra are displayed together with the fits in Fig. 8 and Fig. 9 for 2014 and 2016, respectively. The top row of Fig 7. shows spectra m/Q 34–36 u/e dating from 25.10.2014 15:54 and 26.05.2016 06:08 with black squares and open circles, respectively. The error bars represent the statistical uncertainty. The first spectra of the top row show the detected signal around m/Q 34 u/e. ^{32}S, H_2S, and H_2O_2 can be unambiguously assigned to a part of the measured signal for at least one time period. However, in the case of the 2014 October data, the peak is asymmetric due to possible contributions from $^{16}O^{18}O$ and PH_3. This makes fitting challenging. For this study, it

Downloaded from https://academic.oup.com/mnras/article-abstract/469/Suppl_2/S787/4411814
by Universitaetsbibliothek Bern user
on 20 February 2018

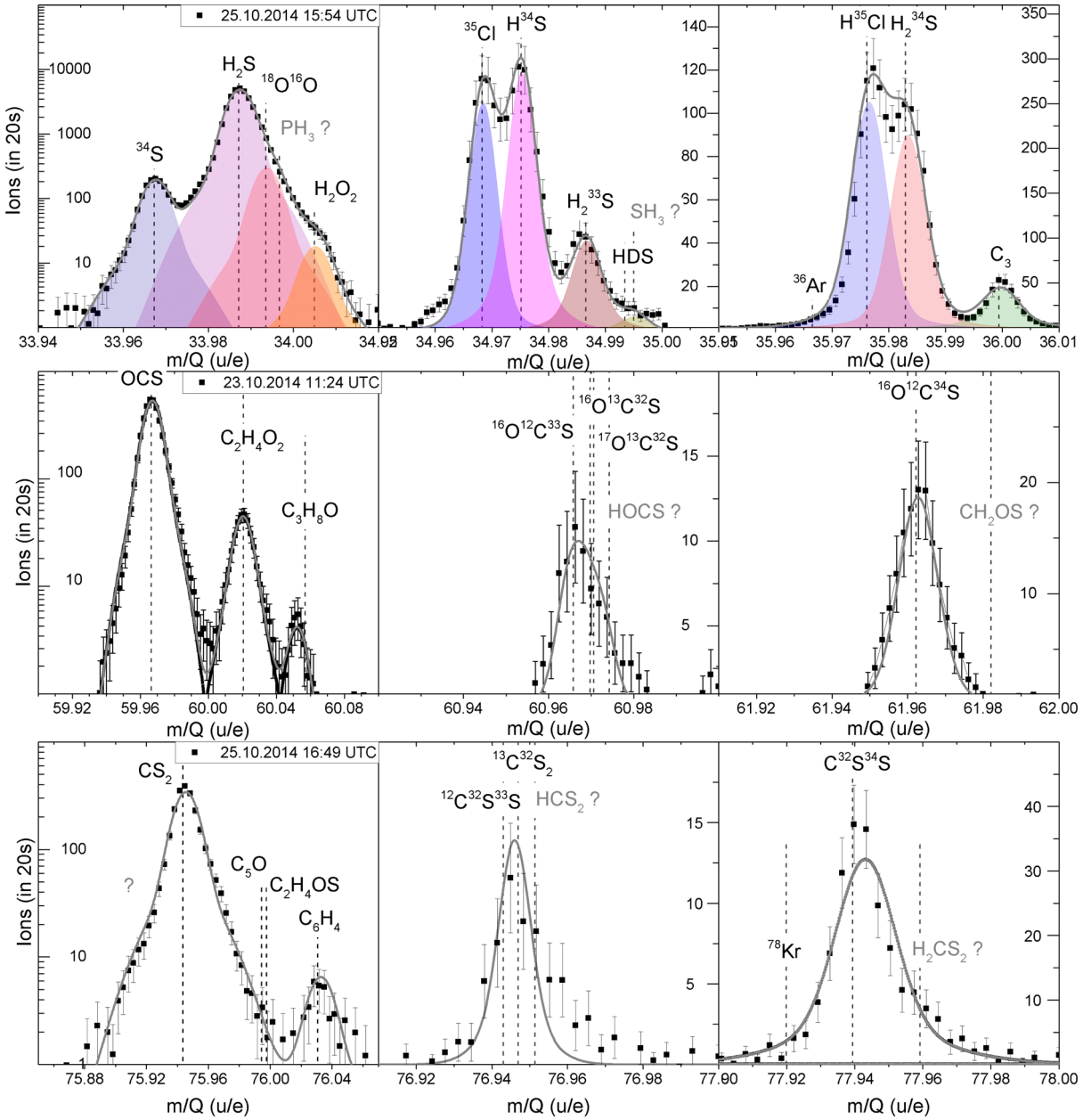

Figure 8. Example spectra of mass-to-charge 34–36 u/e, 60–62 u/e, and 76–78 u/e from 2014 October together with least-squares fit. The fit results are shown as filled area while measurement data are represented by black squares. Identified species are labelled in black while not yet confirmed species are labelled in grey. Error bars solely represent statistical uncertainties.

was assumed that both peaks are possibly present as O_2, with about 4 per cent relative to water, is one of the major gas species in the coma of 67P (Bieler et al. 2015) and because P, a possible fragment of PH_3, has been detected and its origin is not clear yet (Altwegg et al. 2016). In contrast, the spectra from 26.05.2016 06: 08 do not have a feature at the location of H_2O_2 and the peak shape is more symmetric. This can be explained by a smaller amount of O_2 in the coma during this time period. The second spectra in the top row show among others $H_2{}^{33}S$ and HDS around 35 u/e. In addition, there is ^{35}Cl, $H^{34}S$, a fragment of $H_2{}^{34}S$ and potentially some H_3S. The third graph in the first row of Fig. 7 shows the corresponding spectra of 36 u/e. Present are ^{36}Ar (Balsiger et al. 2015), $H^{35}Cl$, $H_2{}^{34}S$, and C_3, most likely a fragment of a hydrocarbon. The peaks of $H_2{}^{34}S$ and $H^{35}Cl$ overlap at almost 90 per cent of the peak height in the case of the data from 25.10.2014 while on 26.05.16 $H^{35}Cl$ is present only on a 10 per cent level of the $H_2{}^{34}S$ peak.

For OCS, example spectra for $m/Q = 60$, 61 and 62 u/e are shown in the middle row of Fig. 7. The filled squares represent the data with highest signal for OCS in 2014 October measured on 23.10.2014 11:24 while the open circles represent typical spectra (25.05.2016 06:38) in 2016 May when *Rosetta* was again at similar distances to 67P as in 2014 October. For the main isotopologues of OCS, no significant interferences with other species are found. However, at per cent level, the peaks of OCS and $C_2H_4O_2$ overlap, which has been taken into account for the least-squares fit. The singly charged ions of the three isotopologues of OCS – $OC^{33}S$, $O^{13}CS$, and ^{17}OCS – have a mass-to-charge of 61 u/e. As a consequence, it is not possible to disentangle the signals of the three isotopologues in DFMS

Downloaded from https://academic.oup.com/mnras/article-abstract/469/Suppl_2/S787/4411814
by Universitaetsbibliothek Bern user
on 20 February 2018

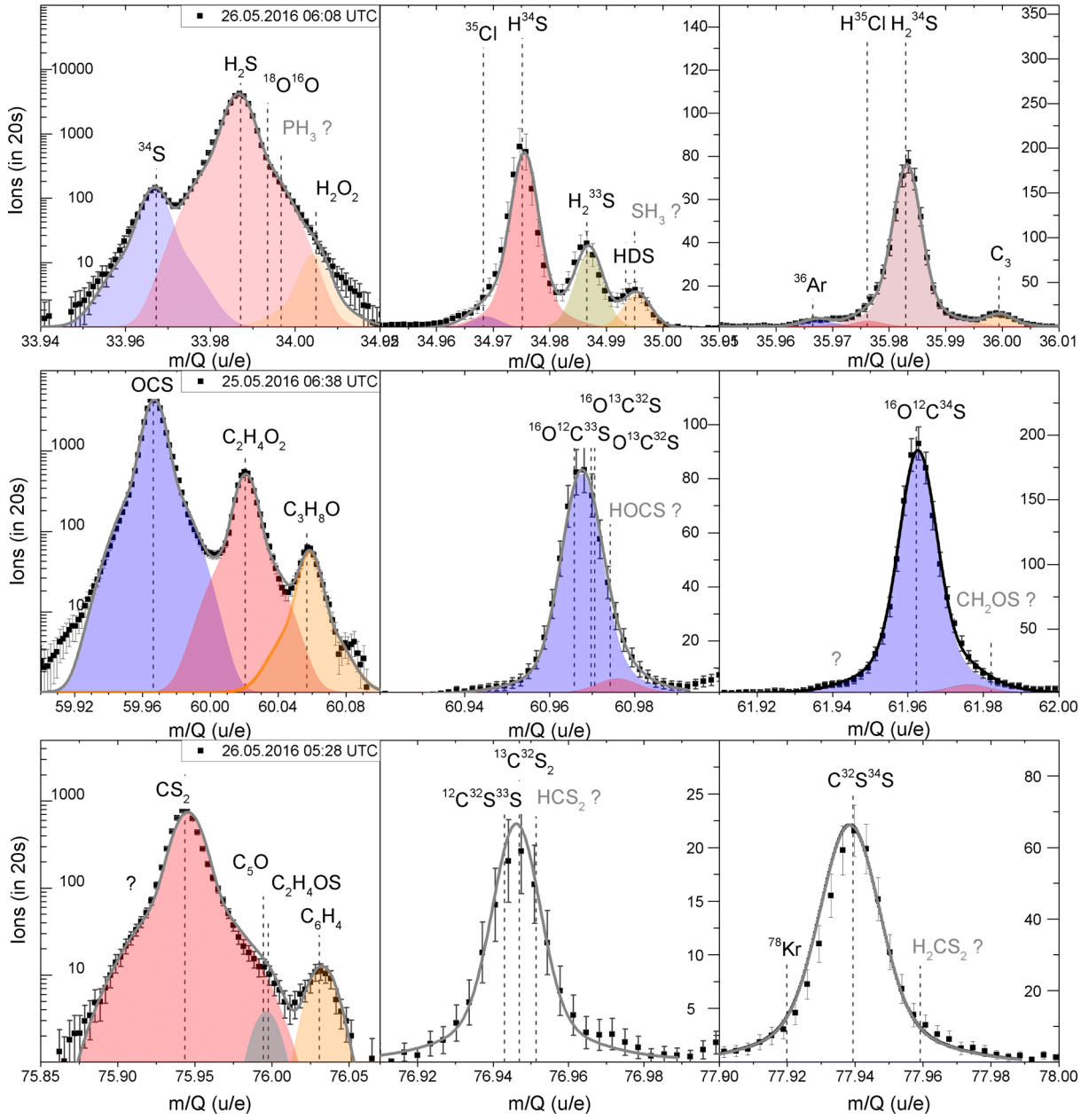

Figure 9. Example spectra of mass-to-charge 34–36 u/e, 60–62 u/e, and 76–78 u/e from 2016 May together with least-squares fit result. The fit results are shown as filled area while measurement data are represented by black squares. Identified species are labelled in black while not yet confirmed species are labelled in grey. Error bars solely represent statistical uncertainty.

spectra as the mass resolution is not sufficient. However, assuming terrestrial isotopic ratios for O, S, and C, the signal of ^{17}OCS can be neglected as its relative abundance compared to OC^{33}S is only 4 per cent. The main contribution is due to O^{13}CS with OC^{33}S being about 79 per cent of O^{13}CS. For this study, the signal of the combined peak has been fitted and the contribution of ^{13}C to the signal ratio $\frac{^{16}O^{12}C^{32}S}{^{16}O^{12}C^{33}S+^{16}O^{13}C^{32}S}$ has been subtracted assuming ^{13}C/^{12}C to be as the standard Vienna Pee Dee Belemnite (V-PDB, Table 1). The second graph in the middle row of Fig. 7 shows the corresponding spectra at 61 u/e, and it can be seen that for 2014 October the combined peak of the OCS isotopologues is around 10 counts leading to a considerable statistical uncertainty for the resulting isotopic ratios, while for 2016 May the signal strength is sufficient for a meaningful determination of ^{33}S/^{32}S. OC^{34}S is the dominant peak at m/Q 62 u/e as it can be seen from the third spectra in the middle row in Fig. 7. The bottom row in this figure shows example spectra of the isotopologues of CS_2 dating from 25.10.2014 15:46 and 26.05.2016 05:28. On the right-hand side of the ^{12}C^{32}S$_2$ peak, a small signal of C_5O and/or C_2H_4OS is present, but only for the 2014 October data as in 2016 May the signal strength in general was lower, as seen in the first graph of the bottom row. In addition, the peak of ^{12}C^{32}S$_2$ displays some asymmetry and it seems as if another species is present on the left-hand side at about $m/Q = 75.92$ u/e. However, no singly or doubly charged ions could be attributed to this mass-to-charge ratio. Similar to OCS, the signal of ^{12}C^{33}S^{32}S and ^{13}C^{32}S$_2$ cannot be distinguished by DFMS and to determine the

Downloaded from https://academic.oup.com/mnras/article-abstract/469/Suppl_2/S787/4411814
by Universitaetsbibliothek Bern user
on 20 February 2018

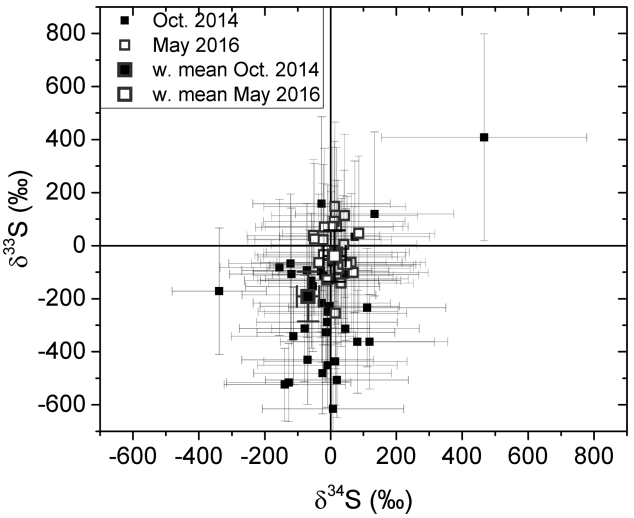

Figure 10. Deviation in the ratio of $^{33}S/^{32}S$ and $^{34}S/^{32}S$ from the standard V-CDT in per mill for H_2S.

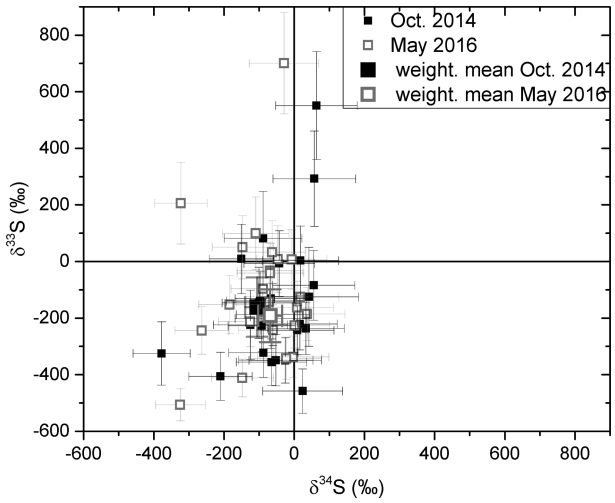

Figure 11. Deviation in the ratio of $^{33}S/^{32}S$ and $^{34}S/^{32}S$ from the standard V-CDT in per mill for CS_2.

$^{33}S/^{32}S$ ratio we again assumed $^{13}C/^{12}C$ to be equal to V-PDB. On mass-to-charge 78 u/e, the $^{12}C^{34}S^{32}S$ peak most likely has on the left-hand side an interference with ^{78}Kr.

Although S, SO, S_2, and SO_2 were detected in the coma of 67P (Calmonte et al. 2016), it was not possible to determine their isotopic ratios. It has been shown by Calmonte et al. (2016) that S and SO are both species present as parents in the coma. However, part of the signal measured by the MCP is due to the fragmentation of other S-bearing molecules by electron impact in the ion source of the instrument. In consequence, the fragmentation pattern of molecules leading to S and SO has to be known specifically for this instrument to retrieve accurate isotopic ratios for S and SO. Presently, these fragmentation patterns are not available with the required accuracy. In the case of S_2 and SO_2, the signal strength of the minor isotopologues is not sufficient to determine isotopic ratios based on single spectra analysis. In 2014 October, the statistical uncertainties of $^{33}S^{32}S$ and $^{34}S^{32}S$ are about 80 per cent and 60 per cent, respectively, while for $^{33}S^{16}O_2$ and $^{34}S^{16}O_2$ they are slightly smaller with about 35 per cent and 20 per cent, respectively. Unfortunately, in 2016 May, the signal strength for both species was even lower.

4.2 H_2S

For H_2S, the signal strength during 2014 October and 2016 May was sufficient to determine the isotopic ratios $^{33}S/^{32}S$ and $^{34}S/^{32}S$. The resulting deviations from the standard V-CDT given in per mill are shown in Fig. 10. 2014 October data and its weighted mean (larger symbol) are represented by the black filled squares while 2016 May data and the weighted mean (larger symbol) are represented by the open grey squares. It can be seen that there are two major differences between the two data sets. First, the spread is different. In 2014 October, $\delta^{34}S$ covers −400 ‰ to 120 ‰ with one exception, while 2016 May data are confined to the range of about −50 ‰ to 50 ‰. In 2014 October, $\delta^{33}S$ ranges from −600 ‰ to 200 ‰ while 2016 May data are in between −200 ‰ and 200 ‰.

Secondly, there is a significant difference of the weighted mean values from V-CDT. The weighted means for 2014 October of $\delta^{33}S$ and $\delta^{34}S$ are (-320 ± 32)‰ ($\sigma_{single} = 265$) and (-40 ± 19)‰ ($\sigma_{single} = 113$), respectively. For 2016 May, they are (-40 ± 19)‰ ($\sigma_{single} = 97$) and (12 ± 7)‰ ($\sigma_{single} = 34$), respectively. Considering $2\sigma_{mean}$ boundaries, the 2016 May data seem to be in agreement with V-CDT for ^{34}S while 2014 October data deviate slightly by just a few per mill. In contrast, both data sets are not in agreement with V-CDT for ^{33}S considering $2\sigma_{mean}$ boundaries. The 2016 May data set disagrees only by a few per mill while for 2014 October the deviation is more significant. An overview on the mean isotopic ratios is given in Table 4 .

4.3 CS_2

The deviation from V-CDT for CS_2 for ^{33}S and ^{34}S is shown in Fig. 11. Except for one data point, the 2014 October data range from about −200 ‰ to 80 ‰ in $\delta^{34}S$. In the case of $\delta^{33}S$, almost all the data range from about −500 ‰ to 100 ‰. Except three data points, the 2016 May data are confined in the same ranges as seen

Table 4. Weighted mean of sulphur isotopic ratios measured in H_2S, OCS, and CS_2 in the coma of 67P during 2014 October and 2016 May when *Rosetta* was within about 10 km distance to the nucleus. Both the uncertainty of the weighted mean and the $1\sigma_{single}$ spread of the data set are given.

Species	Measurement period	$^{34}S/^{32}S$ 10^{-2}	σ_{mean} 10^{-2}	σ_{single} 10^{-2}	$^{33}S/^{32}S$ 10^{-3}	σ_{mean} 10^{-3}	σ_{single} 10^{-3}	$\delta^{34}S$ ‰	σ_{mean} ‰	σ_{single} ‰	$\delta^{33}S$ ‰	σ_{mean} ‰	σ_{single} ‰
H_2S	2014 October	4.24	0.08	0.50	5.35	0.26	2.09	−40	19	113	−321	32	265
H_2S	2016 May	4.47	0.31	0.15	7.57	0.15	0.76	12	7	34	−40	19	97
OCS	2014 October	3.98	0.21	0.39	–	–	–	−99	66	87	–	–	–
OCS	2016 May	4.39	0.06	0.14	6.06	0.45	1.89	−5	14	31	−230	58	240
CS_2	2014 October	4.11	0.11	0.15	6.37	0.28	0.74	−69	24	34	−192	35	93
CS_2	2016 May	3.95	0.10	0.15	6.61	0.33	0.83	−108	23	34	−161	42	105

Downloaded from https://academic.oup.com/mnras/article-abstract/469/Suppl_2/S787/4411814
by Universitaetsbibliothek Bern user
on 20 February 2018

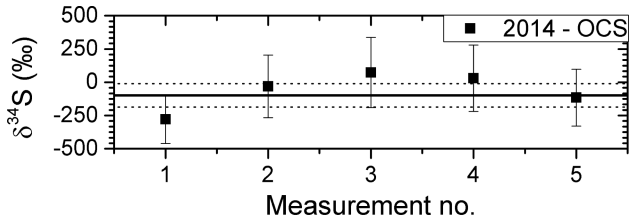

Figure 12. Deviation in the ratio of $^{34}S/^{32}S$ from the standard V-CDT in per mill in OCS during 2014 October.

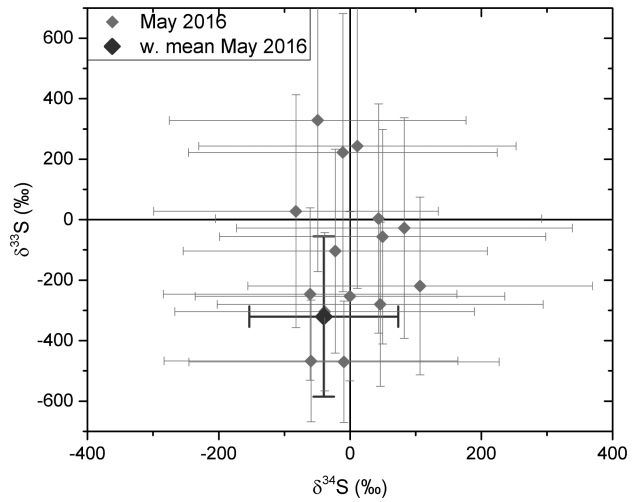

Figure 13. Deviation in the ratio of $^{33}S/^{32}S$ and $^{34}S/^{32}S$ from the standard V-CDT in per mill for OCS.

in 2014 October. Unlike H_2S, the distribution of CS_2 isotopic ratios is not symmetrically distributed around the corresponding standard values. The weighted means for 2014 October data of $\delta^{33}S$ and $\delta^{34}S$ are (-191 ± 35)‰ ($\sigma_{single} = 93$) and (-69 ± 24)‰ ($\sigma_{single} = 34$), respectively. Both data sets are consistent with each other. For 2016 May, they are (-161 ± 42)‰ ($\sigma_{single} = 105$) and (-105 ± 23)‰ ($\sigma_{single} = 34$), respectively. Considering $3\sigma_{mean}$ boundaries 2016 May data are significantly different from V-CDT for both $\delta^{33}S$ and $\delta^{34}S$ while for 2014 October data this only holds for $\delta^{33}S$. However, 2014 October data for $\delta^{34}S$ still disagree with V-CDT when considering $2\sigma_{mean}$ boundaries.

4.4 OCS

As mentioned previously, the signal strength of OCS during 2014 October was not sufficient to determine $\delta^{33}S$. In addition, only tentative values of $\delta^{34}S$ could be determined as a consequence of signal strength and sample size. Fig. 12 shows $\delta^{34}S$ based on five measurements of 2014 October data and the weighted mean of (-99 ± 66)‰ ($\sigma_{single} = 87$). The data range from about -279‰ to 73‰. During 2016 May, the signal strength on the MCP-LEDA was about a factor of 10 higher than in 2014 October allowing the determination of both $\delta^{33}S$ and $\delta^{34}S$ for 16 measurements. The three-isotope plot of the 2016 May data is shown in Fig. 13 together with its weighted mean value. Along $\delta^{34}S$, the data spread between -83 ‰ and 106 ‰ while similar to CS_2 the spread in $\delta^{33}S$ is considerably larger going from -470 ‰ to 329 ‰. The weighted means for 2016 May data of $\delta^{33}S$ and $\delta^{34}S$ are (-230 ± 58)‰ ($\sigma_{single} = 240$) and (-5 ± 14)‰ ($\sigma_{single} = 31$), respectively.

5 DISCUSSION

In the following, the results among molecules in 67P are discussed first and then are put into context with the state-of-the-art knowledge on sulphur fractionation.

In Fig. 14, a compilation of the previously discussed fractionation in SiC grains, comets in general and the results of this study are shown. Meteoritic data were not added as its spread is minuscule around the standard values and would not be seen on this scale. In addition, the mean value for the local interstellar medium (ISM; Chin et al. 1996) has been added. The error bars of our study in the graph represent the uncertainty of the weighted mean (σ_{mean}) while the ellipses in corresponding colour represent $1\sigma_{single}$ of the data set.

There are some differences between the data sets of 2014 October and 2016 May, although heliocentric distances were comparable and in both cases the Sun was on the Northern hemisphere albeit not at the same latitudes. These differences are most probably not intrinsic to the comet, but are due to different contributions from overlapping species. On mass-to-charge ratio 34 u/e, the peaks of $H_2^{32}S$ and ^{32}S both show an asymmetry at the left slope. In addition, this peak shape asymmetry is not present in the corresponding data of 35 u/e and 36 u/e. This implies, that either the asymmetry is in case of 35u/e and 36 u/e smaller than the observed uncertainty due to ion statistics or that the feature only appears on 34u/e. The difference in peak area comparing the left slope of $H_2^{32}S$ of 2014 to 2016 is about 30 per cent. The fit used to determine the peak area, however, did not take into account the asymmetry, and the peak widths between 2014 and 2016 show no significant difference. In consequence, this is not sufficient to explain the differences in $\delta^{33}S$ between the two data sets. The influence of different $^{18}O^{16}O$ and possibly PH_3 abundances relative to H_2S in the two periods to the fits could, however, be a more likely cause. As the difference between 2014 October and 2016 May cannot be unambiguously linked to the interferences with other species on mass-to-charge 34 u/e and as there is a change in peak shape during the course of the mission that is observed for this specific mass-to-charge range, the data set of 2016 May is considered to be less reliable than the one of 2014 October.

In the case of H_2S, 2014 and 2016 data overlap for $\delta^{34}S$ considering $3\sigma_{mean}$. In addition, 2014 is in agreement with V-CDT in the case of $\delta^{34}S$ considering $3\sigma_{mean}$. However, in the case of $\delta^{33}S$ even at $3\sigma_{mean}$ there is no agreement between the data set of 2014 October and 2016 May.

In the case of ^{33}S, there is at $3\sigma_{mean}$ level also no agreement for H_2S with V-CDT for neither of the two data sets.

For CS_2, differences in both $\delta^{33}S$ and $\delta^{334}S$ are small. The two data sets agree within $1(\sigma_{mean})$ as it does for OCS in the case of $\delta^{34}S$.

Considering the assumed bulk relative abundances among the main volatile sulphur-bearing species of $CS_2/H_2S = (0.61 \pm 0.03)$ per cent and $OCS/H_2S = (4.43 \pm 0.16)$ per cent (Calmonte et al. 2016), the mean isotopic composition for volatile sulphur is $\delta^{33}S = (-181 \pm 18)$‰ and $\delta^{34}S = (-16 \pm 10)$‰. However, as discussed in the previous paragraph, the result of 2016 May is considered less reliable than the one from 2014 October. The overall cometary mean isotopic ratio, not considering the results of H_2S from 2016 May, yields $\delta^{33}S = (-302 \pm 29)$‰ and $\delta^{34}S = (-41 \pm 17)$‰.

^{34}S in 67P is comparable to the majority of results in the volatile phase of other comets. Only the two measurements of Hale–Bopp do not overlap considering $1\sigma_{mean}$ boundaries, but only by a small

Downloaded from https://academic.oup.com/mnras/article-abstract/469/Suppl_2/S787/4411814
by Universitaetsbibliothek Bern user
on 20 February 2018

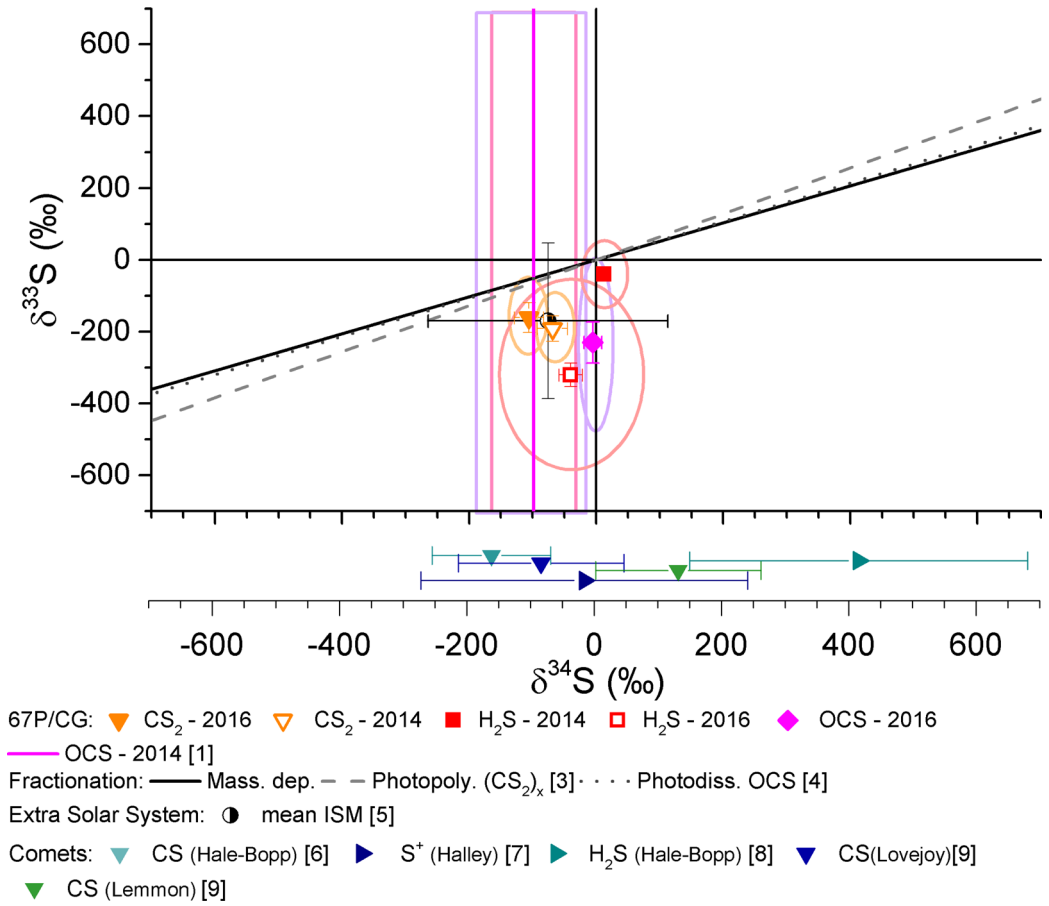

Figure 14. The top panel shows the sulphur three-isotope graph comparing results for 67P with laboratory experiments concerning fractionation induced by photodissociation and the local ISM. The bottom panel shows fractionation of $^{34}S/^{32}S$ in comets. [1] This work, [2] Chakraborty et al. (2013), [3] Zmolek et al. (1999), [4] Lin et al. (2011), [5] Chin et al. (1996), [6] Jewitt et al. (1997), [7] Altwegg (1995), [8] Crovisier et al. (2004), [9] Biver et al. (2016).

amount. In addition, error limits for these measurements are large. For ^{33}S, no data from other comets of the volatile phase are available.

Fractionation can be distinguished into mass-dependent and-independent. From Fig. 14, it can be seen that mass-dependent fractionation is not the main process. Neither can it be due to photodissociation with the current knowledge. Fig. 14 implies that our results are incompatible with photodissociation being the main fractionating process.

The mean bulk isotopic abundance of all sulphur-bearing volatile species is clearly not compatible with the assumed Solar system standard, V-CDT. Most likely, this is not only a chemical effect, but may reflect fractionation between refractory sulphur, where sulphur is mostly in FeS, and volatile sulphur, which might have a different nucleosynthetic origin. A consequence of this would be that the solid and volatile phase sulphur do not share the same reservoir for the formation of molecules. This is supported by the fact that dust impact residuals of comet Wild 2 are very well in agreement with meteoritic sulphur data (Heck et al. 2012). Another possibility is that the material from which the so far sampled comets were formed has not been homogenized prior to incorporation.

Analysis of sulphur isotope fractionation in the different volatile molecules of 67P shows generally some enrichment for ^{32}S with what is assumed as standard value for the Solar system. The fractionation observed is not following the trend expected for photolysis as has been observed in laboratory studies and can also not be explained by mass-dependent fractionation. The difference between different sulphur-bearing molecules is therefore most likely a chemical fractionation effect. The pathway to H_2S is explained by adsorption of positively charged S^+ or HS^+ to negatively charged dust grains in molecular clouds and subsequent addition of H (Ruffle et al. 1997). CS_2 and OCS may be the result of dust grain chemistry or radiolysis of H_2S on the grains. While the adsorption of S^+ or HS^+ on dust grains most likely does not or only slightly fractionate, effects of subsequent radiolysis and desorption may well lead to additional fractionation. The sulphur-bearing species detected in the comet, S_2, S_3, S_4, and the many organosulphurs (Calmonte et al. 2016) show that dust grain chemistry played an important role.

Surprisingly, a comparable degree of fractionation of the sulphur isotopes is present in SiC grains that represent rather the sulphur isotopic composition of stellar outflows than of the molecular cloud from which the Solar system emerged. However, only the AB-type SiC grains are useful candidates as they are supposed to represent the isotopic composition of the material from which the star formed. So far one study was performed with AB SiC grains (Fujiya et al. 2013) and majority is within agreement of meteoritic data (Fig. 2).

Sulphur isotopes were never measured directly in the Sun or solar wind. The best analogue to the solar value was deduced from the CDT meteorite and because inside this meteorite variations in the isotopic composition were detected, a new standard V-CDT was established (Ding et al. 2001). The deviation from solar could therefore in principle also mean that meteoritic sulphur isotopes do not match solar sulphur. This however would be hard to

Downloaded from https://academic.oup.com/mnras/article-abstract/469/Suppl_2/S787/4411814
by Universitaetsbibliothek Bern user
on 20 February 2018

explain. ROSINA has detected a non-solar isotopic ratio for xenon (Marty 2017) as well as for Si (Rubin 2017) in comet 67P, which points to a non-homogeneously mixed protosolar nebula. In addition, a high D_2O/HDO versus HDO/H_2O ratio (Altwegg 2017) and molecular oxygen, which seems to be very well embedded in water (Bieler et al. 2015), have been measured in the coma of 67P. All these observations point to the survival of pre-solar ice into comets and to a heterogeneous protoplanetary nebula. The deviation of the bulk sulphur isotopic abundances in volatiles adds to this picture.

6 CONCLUSION

We report the first detection of $^{33}S/^{32}S$ in cometary volatiles. The ratio could be deduced for H_2S and CS_2. In addition, for both molecules and OCS, the $^{34}S/^{32}S$ ratio could be determined. Taking into account the relative abundances of the sulphur-bearing species (Calmonte et al. 2016), a mean isotopic ratio for the volatile part of 67P of $\delta^{33}S = (-302 \pm 29)‰$ and $\delta^{34}S = (-41 \pm 17)‰$ results. Furthermore, it is the first time that the sulphur fractionation could be detected in several cometary volatiles for the same comet at the same time.

The observed isotopic fractionation in H_2S, CS_2, and OCS does not agree with V-CDT (assumed solar), neither with mass-dependent fractionation nor mass-independent due to photodissociation. It has been concluded that the difference between solid and volatile phase points to a not-homogenized protosolar nebula from which comets are thought to have emerged. This is supported by the detection of non-solar isotopic ratio for xenon (Marty 2017) and Si (Rubin 2017) in comet 67P by ROSINA.

The difference in degree of fractionation among H_2S, CS_2 and OCS is thought to be due to chemical reactions as it cannot be solely linked to mass-dependent nor photo-induced MIF.

ACKNOWLEDGEMENTS

ROSINA would not give such outstanding results without the work of the many engineers, technicians and scientists involved in the mission, in the *Rosetta* spacecraft, and in the ROSINA instrument team over the last 20 years, whose contributions are gratefully acknowledged. *Rosetta* is a European Space Agency (ESA) mission with contributions from its member states and NASA. We acknowledge herewith the work of the whole ESA *Rosetta* team.

Funding: Work at University of Bern was funded by the State of Bern, the Swiss National Science Foundation and the ESA PRODEX (PROgramme de Développement d'Expériences scientifiques) programme. Work at BIRA-IASB was supported by the Belgian Science Policy Office via PRODEX/ROSINA PEA90020 and 4000107705 and by the F.R.S.-FNRS grant PDR T.1073.14 'Comparative study of atmospheric erosion'. Research at Southwest Research Institute is funded by NASA through JPL contract no.196541. This work has been carried out thanks to the support of the A∗MIDEX project (no. ANR-11-IDEX-0001-02) funded by the 'Investissements d'Avenir' French Government programme, managed by the French National Research Agency (ANR). This work was supported by CNES (Centre National d'Etudes Spatiales) grants at LATMOS (Laboratoire Atmosphères, Milieux, Observations Spatiales). Work at the University of Michigan was funded by the US *Rosetta* Project under JPL contract no.1266313. UC thanks Peter Hoppe and James Lyon for the fruitful discussions on silicon carbide grains and the effects of photodissociation on isotopic ratios, respectively.

REFERENCES

Altwegg K., 1995, Habilitation thesis, University of Bern, Bern
Altwegg K., 2017, Phil. Trans. R. Soc. A, 375, 20160253
Altwegg K. et al., 2015, Science, 347, 1261952
Altwegg K. et al., 2016, Sci. Adv., 2, e1600285
Amari S., Hoppe P., Zinner E., Lewis R. S., 1995, Meteoritics, 30, 679
Antonelli M. A. et al., 2014, Proc. Natl. Acad. Sci., 111, 17749
Balsiger H. et al., 2007, Space Sci. Rev., 128, 745
Balsiger H. et al., 2015, Sci. Adv., 1, e1500377
Berthelier J.-J., Illiano J.-M., Nevejans D., Neefs E., Arijs E., Schoon N., 2002, Int. J. Mass Spectrom., 215, 89
Besmehn A., Hoppe P., 2003, Geochim. Cosmochim. Acta, 67, 4693
Bieler A. et al., 2015, Nature, 526, 678
Biver N. et al., 2008, LPI Contrib., 1405, 8146
Biver N. et al., 2016, A&A, 589, A78
Brownlee D. et al., 2006, Science, 314, 1711
Bullock E. S., McKeegan K. D., Gounelle M., Grady M. M., Russel S. S., 2010, Meteorit. Planet. Sci., 45, 885
Calmonte U. et al., 2016, MNRAS, 462, S253
Chakraborty S., Jackson T. L., Ahmed M., Thiemens M. H., 2013, Proc. Natl. Acad. Sci., 110, 17650
Chin Y.-N., Henkel C., Whiteoak J. B., Langer N., Churchwell E. B., 1996, A&A, 305, 960
Crovisier D., Bockelee-Morvan D., Colom P., Biver N., Despois D., Lis D. C., the Team for target-of-opportunity radio observations of comets, 2004, A&A, 418, 1141
Ding T., Valkiers S., Kipphardt H., De Bièvre P., Taylor P. D. P., Gonfiantini R., Krouse R., 2001, Geochim. Cosmochim. Acta, 65, 2433
Farquhar J., Jackson T. L., Thiemens M. H., 2000, Geochim. Cosmochim. Acta, 64, 1819
Franz H. B., Farquhar J., Irving A. J., 2010, LPI Contrib., 1533, 2341
Fujiya W., Hoppe P., Zinner E., Pignatari M., Herwig F., 2013, ApJ, 776, L29
Gao X., Thiemens M. H., 1991, Geochim. Cosmochim. Acta, 55, 2671
Gao X., Thiemens M. H., 1993a, Geochim. Cosmochim. Acta, 57, 3159
Gao X., Thiemens M. H., 1993b, Geochim. Cosmochim. Acta, 57, 3171
Goesmann F. et al., 2015, Science, 349, aab0689
Gyngard F., Nittler L. R., Zinner E., 2010, Meteorit. Planet. Sci. Suppl., 73, 5242
Heck P. R., Hoppe P., Huth J., 2012, Meteorit. Planet. Sci., 47, 649
Hoppe P., Annen P., Strebel R., Eberhardt P., Gallino R., Lugaro M., Amari S., Lewis R. S., 1997, ApJ, 487, L101
Hoppe P., Leitner J., Gröner E., Marhas K. K., Meyer B. S., Amari S., 2010, ApJ, 719, 1370
Hoppe P., Fujiya W., Zinner E., 2012, ApJ, 745, L26
Hoppe P., Lodders K., Fujiya W., 2015, Meteorit. Planet. Sci., 50, 1122
Jewitt D. C., Matthews H. E., Owen T., Meier R., 1997, Science, 278, 90
Kaplan I. R., Hulston J. R., 1966, Geochim. Cosmochim. Acta, 30, 479
Le Roy L. et al., 2015, A&A, 583, A1
Lin Y., Sim M. S., Ono S., 2011, Atmos. Chem. Phys. Discuss., 11, 14233
McSween H. Y., Riciputi L. R., Paterson B. A., 1997, Meteoritics, 32, 51
Marty B., 2017, Science, 356, 1069
Masterson A. L., Farquhar J., Wing B. A., 2011, Earth Planet. Sci. Lett., 306, 253
Monster J., Anders E., Thode H. G., 1965, Geochim. Cosmochim. Acta, 29, 773
Nevejans D., Neefs E., Kavadias S., Merken P., Hoof C. V., 2002, Int. J. Mass Spectrom., 215, 77
Orthous-Daunay F.-R., Gyngard F., Moynier F., Zinner E., 2012, LPI Contrib., 1659, 2679
Rai V. K., Jackson T. L., Thiemens M. H., 2005, Science, 309, 1062
Rubin M., 2017, A&A, 601, A123
Ruffle D. P., Hartquist T. W., Taylor S. D., Williams D. A., 1997, MNRAS, 291, 235
Schläppi B. et al., 2010, J. Geophys. Res.: Space Phys., 115, A12313
Scholten F., Preusker F., Jorda L., Hviid S., 2015, NASA Planetary Data System and ESA Planetary Science Archive

Downloaded from https://academic.oup.com/mnras/article-abstract/469/Suppl_2/S787/4411814
by Universitaetsbibliothek Bern user
on 20 February 2018

Werner R. A., Brand W. A., 2001, Rapid Commun. Mass Spectrom., 15, 501
Woods P. M., Occhiogrosso A., Viti S., Kaňuchová Z., Palumbo M. E., Price S. D., 2015, MNRAS, 450, 1256
Wright I. P., Sheridan S., Barber S. J., Morgan G. H., Andrews D. J., Morse A. D., 2015, Science, 349
Xu Y., Zinner E., Gallino R., Heger A., Pignatari M., Lin Y., 2015, ApJ, 799, 156
Zinner E., 1998, Meteorit. Planet. Sci., 33, 549
Zinner E., 2007, in Holland H. D., Turekian K. K., eds., Treatise on Geochemistry. Pergamon, Oxford, p. 1
Zinner E., 2014, in Holland H. D., Turekian K. K., eds, Treatise on Geochemistry, 2nd edn. Elsevier, Oxford, p. 181
Zmolek P., Xu X., Jackson T., Thiemens M. H., Trogler W. C., 1999, J. Phys. Chem. A, 103, 2477

APPENDIX A: OVERVIEW OF METEORITIC STUDIES ON SULPHUR ISOTOPES

A1 Ordinary meteorites

A1.1 Chondrites

For seven carbonaceous meteorites, sulphur isotopic measurements of soluble and insoluble organic compounds were done by Gao & Thiemens (1993a, Fig. 1). They reported internal sulphur isotopic composition variations, and all results are consistent with mass-dependent fractionation. Internal variations in δ^{34}S, relative to CDT, were reported for Orgueil (CI; ∼6.5 ‰ to 7.1 ‰), Murchison (CM; ∼3 ‰ to 8.5 ‰), and Mighei, ALHA84029 (∼8.36 ‰).

Besides carbonaceous meteorites, Gao & Thiemens (1993b) also studied ordinary and enstatite chondrites for their sulphur isotopic composition. For the ordinary chondrites Bjurbole and Chainpur, the variation in δ^{34}S between matrices and chondrules is 0.14‰ and 0.91‰. However, in Bjurbole, chondrules possess the heavy isotopic composition while in Chainpur, the matrices are the carrier of the heavy isotopic composition which was suggested to be the result of either the process of chondrule formation or the chondrules formed from two distinct reservoirs. For the enstatite meteorites Abee, Qingzhen, and Indarch, internal isotopic variations in the range of 0.2‰ to 2.0‰ are reported which may be a sign for regional heterogeneity in the solar nebula. Apart from studying meteorite internal variations, Gao & Thiemens (1993b) pointed out that between different chondrite groups there is a difference in δ^{34}. Going from depletion relative to CDT to enrichment, the average δ^{34}S are for enstatite (-0.26 ± 0.07) ‰, ordinary chondrites (-0.02 ± 0.06) ‰, and carbonaceous chondrites (0.49 ± 0.16) ‰.

A thorough study of sulphur isotopic composition in Fe–Ni sulphide grains in two CI and six CM carbonaceous chondrites has been done by Bullock et al. (2010) using secondary ion mass spectrometry (SIMS), which allows one to do petrographic analysis before and after isotopic analysis. Thus, the matrix type can be verified unambiguously after the measurement, unlike in the study of Gao & Thiemens (1993a), where chemical extraction and gas mass spectrometry were used. Remarkably, Bullock et al. (2010) obtained different results for the range of enrichment and depletion of large (∼300 μm) sulphide grains in chondrules embedded in the matrix and in the rim while previous studies (Monster, Anders & Thode 1965; Kaplan & Hulston 1966; Gao & Thiemens 1993a) showed only an enrichment in δ^{34}S for CI chondrites. For CM chondrites, the majority of grains showed in average a depletion of δ^{34}S $= -0.9$ ‰ while McSween, Riciputi & Paterson (1997) reported an enrichment in sulphide grains of Kaidun (CM1). A possible cause for the inconsistency is a bias in the samples since in this study nanophase sulphide grains and sulphur-bearing minerals could not be measured, although they might have been part of the sample for previous studies where they were extracted chemically (Bullock et al. 2010).

A1.2 Achondrites

Achondrites have been studied for their sulphur isotopic composition by Rai et al. (2005) revealing an enrichment in ^{33}S in sulphides. In their study, they extracted sulphide phases from four groups [howardite-eucrite-diogenite (HEDs), acapulcoite-lodranites, aubrites, ureilites, and two ungrouped ones] and measured the isotopic composition. In this set, HEDs, acapulcoite-lodranites and aubrites show an enrichment in ^{33}S of δ^{33}S $= 0.227 \pm 0.049$‰, δ^{33}S $= 0.034 \pm 0.028$‰, and δ^{33}S $= 0.119 \pm 0.167$‰, respectively and an enrichment as well in ^{34}S δ^{34}S $= 0.373 \pm 0.170$‰, δ^{34}S $= 0.015 \pm 0.147$‰, and δ^{34}S $= 0.319 \pm 0.747$‰, respectively (with respect to CDT). Cosmic spallation and stellar nucleosynthesis are ruled out as the source of the enrichment because (i) achondrites do not have enough target Fe and too short cosmic ray exposure ages to produce the needed amount of ^{33}S through spallation, (ii) ^{36}S/^{32}S is constant within the uncertainties of the measurements while ^{32}S/^{33}S and ^{32}S/^{34}S are not constant which cannot be the case since ^{32}S, ^{33}S, and ^{34}S are produced in similar star types while ^{36}S is not and since 36 is the least abundant, its isotopic ratio is very sensitive to changes.

A1.3 Ureilites

Farquhar et al. (2000) analysed 22 samples from 17 ureilites, a type of chondritic meteorite, for their sulphur isotopic composition and reported a small enrichment in ^{33}S relative to carbonaceous chondrites. The average was δ^{34}S $= (0.44 \pm 0.30)$‰ (1σ) and δ^{33}S $= (0.28 \pm 0.15)$‰ relative to CDT, and their data lay on an MIF line (see Fig. 1). The conclusion was that the enrichment is pristine leaving the question why the ureilite parent body should have a non-chondritic sulphur isotopic composition.

A1.4 Iron meteorites

An excess in ^{33}S and ^{36}S has been reported by Gao & Thiemens (1991) in the metal phase (FeNi alloy) and schreibersite of four iron meteorites, and it has to be accounted as a result of spallogenic nuclear reactions. Sulphur isotopic composition of troilites (FeS) extracted from the same set of iron meteorites was consistent with mass-dependent fractionation.

A2 Possible link between meteorites and photodissociation

Recently, a study on the sulphur isotopic composition of magmatically differentiated meteorites has been published by Antonelli et al. (2014). They investigated the possible processes which could lead to the same isotopic composition as measured in those meteorites. As cause for this study, the authors recall the conclusion drawn by Rai et al. (2005): (i) that the sulphur isotopic composition was not homogeneous among the material which later formed the early Solar system planetesimals, and (ii) the 182Hf-182 ages laying within 1–3 Myr of Solar system formation of magmatic irons implying that those are the oldest rocks formed in the Solar system. Therefore, 61 troilite (FeS) nodules from 58 iron meteorites covering eight

Downloaded from https://academic.oup.com/mnras/article-abstract/469/Suppl_2/S787/4411814
by Universitaetsbibliothek Bern user
on 20 February 2018

different groups (IAB, IC, IIAB, IIE, IIIAB, IIIF, IVA and IVB) have been analysed resulting in (−0.799 to 1.289)‰ for δ^{34}S and δ^{33}S = (−0.562 to 0.532)‰, respectively, leading to a slope of ∼(0.516 ± 0.009)‰. In their report, Antonelli et al. (2014) discuss different possible processes which could lead to the measured δ^{33}S of (0.042 ± 0.007)‰ (magmatic processes, kinetic processes, mixing of distinct reservoirs, and Rayleigh distillation); here, however, we will only debate the impact of nucleosynthesis, cosmic ray exposure and effects of photochemistry.

For Antonelli et al. (2014), nucleosynthesis seems to be unlikely the cause for the variations seen in δ^{36}S and δ^{33}S because (i) nucleosynthesis would affect mostly δ^{33}S since ^{36}S is thought to be produced in different reactions and circumstances than ^{32}S, ^{33}S, and ^{34}S; (ii) a mixture of Solar system reservoir with a reservoir distinguished by a large ^{32}S excess (as it is measured in some SiC grains, see later) would lead to a unidirectional depletion in all minor isotopes. Additionally, the case of injection with such material requires a non-chondritic sulphur isotopic composition at the beginning and that the amount of sulphur carried by the SiC grains is not negligible relative to the total sulphur content in the early Solar system stage. The authors argue against cosmic ray exposure because (i) there is no correlation between exposure age products due to neutrons and the measured sulphur isotopic ratios, and (ii) the slope for δ^{36}S/δ^{33}S obtained in this study diverges from theoretical predictions (δ^{36}S/δ^{33}S ∼ −7 ± 4 and δ^{36}S/δ^{33}S ∼ 8). As a possible cause, Antonelli et al. (2014) suggest gas-phase photochemistry during the T-Tauri phase of the Sun. They assume that H_2S, the most abundant S-bearing gas, is within ∼2 au distance from the Sun and near to the surface of the disc. Due to Lyman α radiation, photolysis of H_2S would occur resulting in an MIF similar to what has been observed for achondritic and iron meteorites. They model the H_2S photolysis with time-dependent mid-plane temperature and disc surface density but isothermal vertical temperature profile. Based on the yield in the laboratory work done by Chakraborty et al. (2013), it is estimated that ∼2 per cent of the total H_2S is photolyzed and present in the region where parent bodies of achondritic and iron meteorites formed. The authors report that it is possible to photolyze ∼2 per cent of H_2S in the time span of the T-Tauri phase for a high-mass and a low-mass (0.24 $M_\odot$) disc type.

A3 Sulphur fractionation in SiC grains

SiCgrains are a type of pre-solar grains which formed in stellar outflows of late-type stars (e.g. red giants) and as condensates of stellar explosions like supernovae (SNe). Based on the their anomalous isotopic ratios in C, S, N, and O, they were identified to not have formed in the Solar system. For a review, see Zinner (2014). Besides the SiC grains, there are seven other types of grains with pre-solar origin identified: diamond, graphite, oxides, silicon nitride, Ti-/Te-/Zr-/Mo-carbides, kamacite/iron, and olivine (Zinner 2007). Before pre-solar grains were embedded in Solar system bodies like meteorites, interplanetary dust particles, Antarctica meteorites, and cometary matter (Xu et al. 2015), they travelled through interstellar matter and were exposed to cosmic galactic rays, could experience sputtering by stellar wind and could be evaporated by SN shocks (Zinner 1998). At some point, they became part of the dense molecular cloud from which our Solar system emerged. Most of those grains were destroyed during the formation process of the Solar system bodies but some survived and preserved their pre-solar signature because they were embedded in almost non-processed bodies like carbonaceous chondrites (e.g. CM2 Murchison).

SiCgrains have been detected already more than 20 years ago and have been studied for their isotopic ratios. Since then, only during the last five years extensive studies of single grains could be done due to improvements of the analysis techniques (Hoppe et al. 2010, 2012, 2015; Xu et al. 2015). Here we concentrate on sulphur isotopic ratios in those grains. Almost all of the presented data were retrieved from SiC grains from Murchison meteorite, which contains on average the largest grain sizes. This makes it possible to examine single grains instead of a collection of grains. Thus, the likely origin of a single grain can be determined from its isotopic ratios.

Based on their Si, C, and N isotopic composition, SiC grains are divided into subcategories (Hoppe et al. 1997): so-called mainstream grains (93 per cent of the total), Y, Z, AB, X, C, possible nova, and U grains (Zinner 2014).

Recently, two studies examined SiC grains from Murchison meteorite for their isotopic composition: C, Si, N, S, Mg–Al, and Ca–Ti isotopic composition by Xu et al. (2015), and Si, C, and S isotopic composition by Hoppe et al. (2015). For their analysis, Xu et al. (2015) used SiC grains of the separate KJE [described by Amari et al. (1995)] which have a typical diameter between 0.5 and 0.8 μm. With the Cameca NanoSIMS 50 ion microprobe, an automatic isotopic imaging was done to find rare SiC grains. The selected grains were then measured with negative ion images to obtain isotopic abundances. They report mass fractionation in ^{33}S and ^{34}S for 16 X grains, 1 C grain, 1 Y grain, 5 Z grains, and 2 silicon nitride grains (Fig. 2). Z, Y, and silicon nitride grains show mass fractionation of ±100 ‰ for ^{34}S and almost no spread for ^{33}S, X grains show a larger spread with ± 200 ‰ and ± 400‰, respectively, whereas the C grain shows the largest depletion in ^{33}S and ^{34}S with (−944 ± 33)‰ and (−941 ± 14)‰, respectively. They conclude that the large ^{32}S excess comes more likely from decay of short-lived ^{32}Si than from the fractionation model by Hoppe et al. (2012) because the excess is larger than what is predicted for the Si/S zone of core-collapse SNe. Besides comparing models of SNe, Xu et al. (2015) addressed two main problems for S isotope studies: first, low intrinsic concentration since S does not readily condense into SiC, and secondly some contamination with isotopically terrestrial S during the separation process. So for the C grain in the negative ion image, most of the S was located at the rim and the depletion was less there than for the centre part (for more details, see Xu et al. 2015). The mean value over the entire image would be δ^{34}S = (−703 ± 14)‰ and δ^{34}S = (−714 ± 24)‰.

Hoppe et al. (2015) studied 14 pre-solar SiC mainstream grains for their C, Si and S isotopic composition. They prepared a 48 g sample of Murchison meteorite following a similar procedure which was used for the separate KJE by Amari et al. (1995) and developed by Besmehn & Hoppe (2003). To minimize the bias in the results due to S contamination, only grains with smooth surface and a compact appearance were selected for this study. Additionally, the grains and their surroundings were cleaned with a Cs^+ ion beam via pre-sputtering. Due to surface topography, not all the surface contamination could be removed. Isotopic abundances were calculated from negative ion measurements of $^{33}S^-$ and $^{34}S^-$. The above-discussed results all are shown in Fig. 2.

Downloaded from https://academic.oup.com/mnras/article-abstract/469/Suppl_2/S787/4411814
by Universitaetsbibliothek Bern user
on 20 February 2018

APPENDIX B: TABLES OF INDIVIDUAL MEASUREMENTS

Table B1. Deviation of $^{33}S/^{32}S$ and $^{34}S/^{32}S$ isotopic ratio from V-CDT in H_2S at 67P during 2014 October.

Measurement time UTC	$^{34}S/^{32}S$ 10^{-2}	Error 10^{-2}	$^{33}S/^{32}S$ 10^{-3}	Error 10^{-3}	$\delta^{34}S$ ‰	Error ‰	$\delta^{33}S$ ‰	Error ‰
20.10.2014 01:33	3.92	0.83	5.19	1.44	−113	189	−341	183
20.10.2014 02:16	4.50	0.96	3.88	1.11	19	217	−507	141
20.10.2014 03:00	4.38	0.94	4.33	1.25	−9	212	−451	159
20.10.2014 03:44	4.38	0.94	7.54	2.14	−8	212	−43	272
20.10.2014 04:27	4.62	0.99	5.41	1.56	45	224	−314	199
20.10.2014 05:10	4.11	0.88	4.49	1.32	−70	200	−431	168
20.10.2014 05:53	4.48	0.96	4.44	1.30	15	218	−437	165
20.10.2014 06:37	4.45	0.95	3.03	0.89	7	215	−615	113
20.10.2014 07:20	4.94	1.05	5.02	1.41	119	238	−362	178
20.10.2014 08:05	4.40	0.93	6.08	1.67	−3	211	−229	212
20.10.2014 08:49	4.35	0.92	5.30	1.48	−14	210	−328	187
23.10.2014 12:06	6.48	1.38	11.1	3.07	467	318	409	390
23.10.2014 12:49	3.80	0.81	3.75	1.08	−139	189	−524	137
23.10.2014 13:33	4.31	0.93	4.09	1.21	−24	209	−481	153
23.10.2014 14:59	4.78	1.03	5.02	1.53	82	234	−363	194
23.10.2014 15:42	4.13	0.90	6.42	1.92	−65	203	−186	244
23.10.2014 16:25	4.32	0.94	6.99	2.06	−22	212	−113	262
23.10.2014 17:08	4.16	0.90	6.83	2.01	−58	204	−132	255
23.10.2014 17:51	3.86	0.83	3.81	1.16	−127	189	−516	147
24.10.2014 00:48	2.92	0.63	6.53	1.88	−338	143	−172	238
24.10.2014 02:14	4.07	0.87	5.41	1.58	−79	198	−313	200
24.10.2014 02:58	4.30	0.92	9.12	2.58	−27	209	158	328
24.10.2014 03:41	4.38	0.94	5.91	1.69	−8	213	−249	215
24.10.2014 14:13	4.30	0.92	6.17	1.77	−27	209	−216	225
24.10.2014 14:56	4.91	1.05	6.03	1.76	111	239	−234	223
24.10.2014 15:39	4.37	0.94	5.60	1.66	−11	214	−289	211
24.10.2014 16:22	4.18	0.90	6.67	1.93	−54	204	−154	245
24.10.2014 19:39	4.62	0.98	7.02	1.95	46	222	−109	248
24.10.2014 20:22	4.10	0.87	7.14	1.99	−72	198	−94	253
24.10.2014 20:43	3.73	0.80	7.23	2.02	−156	180	−82	257
25.10.2014 04:41	4.29	0.91	7.12	1.97	−29	206	−96	251
25.10.2014 05:25	3.88	0.83	7.35	2.06	−122	188	−67	262
25.10.2014 06:09	4.43	0.95	7.38	2.10	2.6	215	−63	266
25.10.2014 15:02	5.01	1.06	8.82	2.44	134	241	120	309
25.10.2014 15:45	4.74	1.01	8.14	2.25	74	228	34	286
25.10.2014 20:55	4.42	0.94	6.84	1.92	0	213	−132	243
26.10.2014 02:02	4.56	0.97	7.27	2.01	33	219	−77	255
26.10.2014 02:46	3.89	0.83	7.03	1.96	−119	188	−107	249

Downloaded from https://academic.oup.com/mnras/article-abstract/469/Suppl_2/S787/4411814
by Universitaetsbibliothek Bern user
on 20 February 2018

Table B2. Deviation of $^{33}S/^{32}S$ and $^{34}S/^{32}S$ isotopic ratio from V-CDT in H_2S at 67P during 2016 May.

Measurement time UTC	$^{34}S/^{32}S$ 10^{-2}	Error 10^{-2}	$^{33}S/^{32}S$ 10^{-3}	Error 10^{-3}	$\delta^{34}S$ ‰	Error ‰	$\delta^{33}S$ ‰	Error ‰
16.05.2016 10:28	4.32	0.92	7.60	2.11	−21	208	−35	269
17.05.2016 12:33	4.26	0.91	7.36	2.04	−36	205	−65	259
18.05.2016 22:54	4.60	0.98	7.91	2.20	41	222	4	279
22.05.2016 16:48	4.80	1.02	8.24	2.30	86	231	46	292
22.05.2016 19:06	4.52	0.96	7.19	2.00	24	218	−87	254
22.05.2016 21:16	4.50	0.97	8.44	2.35	19	217	72	299
22.05.2016 23:30	4.72	1.00	7.07	1.96	69	227	−102	249
23.05.2016 01:53	4.50	0.96	6.89	1.93	19	217	−126	245
24.05.2016 10:52	4.18	0.89	8.17	2.26	−53	201	37	287
24.05.2016 14:05	4.69	1.00	7.38	2.04	63	226	−63	259
24.05.2016 16:14	4.20	0.90	8.07	2.25	−49	203	24	285
24.05.2016 18:26	4.58	0.98	7.32	2.04	38	221	−71	260
24.05.2016 19:03	4.37	0.93	6.86	1.91	−11	211	−130	243
24.05.2016 21:22	4.47	0.95	8.59	2.38	11	215	91	302
26.05.2016 05:24	4.47	0.95	7.54	2.11	11	216	−43	268
26.05.2016 06:08	4.44	0.95	8.44	2.36	5	214	72	300
26.05.2016 07:02	4.47	0.95	7.68	2.14	13	216	−25	272
26.05.2016 09:21	4.33	0.92	8.42	2.35	−19	209	69	298
26.05.2016 11:21	4.32	0.92	8.05	2.23	−22	208	22	284
26.05.2016 13:20	4.56	0.97	6.76	1.89	32	220	−141	239
26.05.2016 15:20	4.64	0.99	7.31	2.03	50	223	−72	257
27.05.2016 18:14	4.61	0.98	8.76	2.42	43	222	113	308
28.05.2016 00:13	4.47	0.95	9.04	2.51	13	216	147	319
28.05.2016 01:38	4.51	0.96	7.68	2.13	22	217	−25	271
28.05.2016 03:46	4.48	0.96	5.87	1.65	15	216	−255	209

Table B3. Deviation of $^{33}S/^{32}S$ and $^{34}S/^{32}S$ isotopic ratio from V-CDT in CS_2 at 67P during 2014 October.

Measurement time UTC	$^{34}S/^{32}S$ 10^{-2}	Error 10^{-2}	$^{33}S/^{32}S$ 10^{-3}	Error 10^{-3}	$\delta^{34}S$ ‰	Error ‰	$\delta^{33}S$ ‰	Error ‰
21.10.2014 19:24	4.36	1.93	5.42	2.60	−12	437	−312	330
21.10.2014 20:08	4.29	1.90	8.19	3.91	−30	429	40	496
21.10.2014 20:51	3.80	1.68	8.32	3.98	−139	381	56	506
21.10.2014 23:33	4.19	1.85	5.37	2.58	−52	420	−319	327
22.10.2014 00:25	4.18	1.85	7.19	3.45	−54	419	−88	438
22.10.2014 04:43	4.18	1.85	6.61	3.18	−54	420	−161	404
22.10.2014 05:25	4.56	2.02	8.27	3.96	32	456	50	503
22.10.2014 06:10	4.04	1.79	7.12	3.40	−85	405	−97	432
22.10.2014 06:53	4.52	2.00	6.28	3.00	23	452	−203	380
22.10.2014 13:45	4.76	2.11	12.7	6.09	78	478	613	773
22.10.2014 14:29	4.55	2.01	6.46	3.09	30	455	−180	392
22.10.2014 15:13	4.08	1.81	5.64	2.71	−76	410	−284	344
22.10.2014 21:03	4.06	1.80	6.41	3.07	−80	407	−186	389
23.10.2014 18:11	4.03	1.79	7.06	3.43	−88	406	−103	436
23.10.2014 18:54	3.54	1.57	4.96	2.40	−199	356	−370	305
23.10.2014 19:38	4.73	2.10	10.6	5.11	72	476	348	648
23.10.2014 20:21	3.92	1.75	6.44	3.15	−113	396	−183	400
24.10.2014 01:08	2.78	1.25	5.62	2.76	−370	283	−287	351
24.10.2014 01:51	4.08	1.82	8.91	4.35	−77	412	131	552
24.10.2014 03:17	4.24	1.88	5.42	2.62	−39	426	−312	333
24.10.2014 04:00	4.20	1.87	6.72	3.24	−48	422	−146	412
25.10.2014 05:01	4.73	2.10	7.56	3.65	70	475	−40	463
25.10.2014 16:49	4.58	2.03	4.54	2.20	38	461	−424	280
25.10.2014 17:32	4.63	2.05	6.33	3.03	47	463	−196	385
26.10.2014 03:49	4.66	2.10	7.23	3.65	56	476	−82	463

Downloaded from https://academic.oup.com/mnras/article-abstract/469/Suppl_2/S787/4411814
by Universitaetsbibliothek Bern user
on 20 February 2018

Table B4. Deviation of $^{33}S/^{32}S$ and $^{34}S/^{32}S$ isotopic ratio from V-CDT in CS_2 at 67P during 2016 May.

Measurement time UTC	$^{34}S/^{32}S$ 10^{-2}	Error 10^{-2}	$^{33}S/^{32}S$ 10^{-3}	Error 10^{-3}	$\delta^{34}S$ ‰	Error ‰	$\delta^{33}S$ ‰	Error ‰
24.05.2016 07:21	3.95	1.74	7.00	3.32	−106	394	−111	422
24.05.2016 11:49	3.92	1.73	6.53	3.11	−113	392	−172	395
24.05.2016 13:37	4.51	1.99	6.93	3.30	22	451	−120	419
24.05.2016 15:02	3.30	1.46	6.27	2.99	−254	330	−204	380
24.05.2016 17:11	3.65	1.62	7.01	3.36	−173	366	−110	426
24.05.2016 20:09	4.27	1.89	8.31	3.97	−34	427	55	504
24.05.2016 22:19	3.82	1.69	8.65	4.11	−135	382	99	522
26.05.2016 05:44	3.03	1.34	9.91	4.74	−314	304	259	602
26.05.2016 06:27	4.56	2.02	7.23	3.47	32	457	−82	441
26.05.2016 07:37	3.81	1.69	4.92	2.34	−136	382	−376	298
26.05.2016 09:41	3.99	1.76	9.05	4.32	−97	399	149	549
26.05.2016 11:41	4.46	1.97	5.52	2.63	10	446	−300	334
26.05.2016 13:40	4.21	1.86	6.28	3.00	−48	421	−203	381
26.05.2016 17:50	4.16	1.83	7.10	3.37	−58	415	−99	428
27.05.2016 11:28	4.17	1.84	7.98	3.79	−56	416	13	481
27.05.2016 18:34	4.17	1.84	7.91	3.77	−56	417	5	478
27.05.2016 20:33	4.45	1.96	8.30	3.94	7	444	54	501
27.05.2016 22:33	4.35	1.92	13.9	6.61	−16	435	767	839
28.05.2016 00:32	4.64	2.05	6.74	3.22	51	464	−144	409
28.05.2016 01:57	4.38	1.93	5.47	2.61	−9	438	−305	332
28.05.2016 04:06	3.02	1.34	4.15	1.98	−316	303	−474	251
28.05.2016 06:06	4.19	1.85	8.51	4.05	−50	419	81	514
28.05.2016 08:05	4.48	1.98	6.41	3.04	15	448	−186	386
30.05.2016 23:25	4.08	1.80	7.47	3.54	−77	407	−52	450

Table B5. Deviation of $^{33}S/^{32}S$ and $^{34}S/^{32}S$ isotopic ratio from V-CDT in OCS at 67P during 2016 May.

Measurement time UTC	$^{34}S/^{32}S$ 10^{-2}	Error 10^{-2}	$^{33}S/^{32}S$ 10^{-3}	Error 10^{-3}	$\delta^{34}S$ ‰	Error ‰	$\delta^{33}S$ ‰	Error ‰
12.05.2016 13:14	4.62	1.10	5.67	2.14	46	248	−280	272
14.05.2016 07:35	4.20	1.00	10.5	3.94	−49	226	329	500
15.05.2016 11:56	4.89	1.16	6.15	2.32	107	262	−219	294
15.05.2016 12:39	4.64	1.10	7.44	2.79	50	249	−56	355
16.05.2016 18:54	4.32	1.02	7.06	2.65	−22	232	−104	337
19.05.2016 06:22	4.61	1.10	7.91	2.99	44	248	4	379
25.05.2016 06:38	4.78	1.13	7.66	2.87	83	256	−28	365
25.05.2016 11:26	4.15	0.99	5.94	2.24	−61	224	−246	285
25.05.2016 19:01	4.25	1.01	5.48	2.06	−39	228	−304	262
27.05.2016 03:51	4.38	1.04	4.17	1.58	−9	236	−470	201
27.05.2016 11:21	4.15	0.99	4.20	1.59	−60	224	−467	201
27.05.2016 13:25	4.05	0.96	8.10	3.03	−83	217	28	385
27.05.2016 14:18	4.42	1.04	5.88	2.20	0	236	−253	280
27.05.2016 16:28	4.37	1.04	9.63	3.62	−11	235	222	460
28.05.2016 07:58	4.47	1.07	9.80	3.71	11	242	244	471

This paper has been typeset from a TEX/LATEX file prepared by the author.

Downloaded from https://academic.oup.com/mnras/article-abstract/469/Suppl_2/S787/4411814
by Universitaetsbibliothek Bern user
on 20 February 2018